ANALYSIS OF CALORIMETER/ITC COSMIC RAY DATA FROM THE ATLAS DETECTOR, AND PREPARATION FOR SUPERSYMMETRY SEARCHES

by

CARLOS FRANCISCO MEDINA HERNANDEZ

Presented to the Faculty of the Graduate School of

The University of Texas at Arlington in Partial Fulfillment

of the Requirements

for the Degree of

MASTER OF SCIENCE IN PHYSICS

THE UNIVERSITY OF TEXAS AT ARLINGTON

May 2009

ACKNOWLEDGEMENTS

I want to thank my advisor Andy White, for his guidance and advice. I extend my gratitude to Kaushik De for his unconditional support. Also thanks very much to my mom, my dad, and my brother for their dedication and love. Finally thanks to Heather for all the support she has always provided.

April 20, 2009

ABSTRACT

ANALYSIS OF CALORIMETER/ITC COSMIC RAY DATA FROM THE ATLAS DETECTOR, AND PREPARATION FOR SUPERSYMMETRY SEARCHES

Carlos Francisco Medina, M.S

The University of Texas at Arlington, 2009

Supervising Professor: Andrew White

The Large Hadron Collider is the largest most ambitious experiment in high energy physics history. It involves the greatest number of scientists from around the world. The first collisions will start being produced in late 2009 and we expect that the information collected will help us understand the physics behind the standard model such as higgs physics and the supersymmetric theories. The Department of Physics at University of Texas at Arlington, and more specifically the high energy physics group is actively involved with the design, construction and commissioning process of the ATLAS Tile Calorimeter. The group is also participating in the ATLAS computational network, or Grid, with the installation of a Tier2 computing center at UTA campus. This work presents some of the commissioning tasks performed in the summers of 2006 and 2007, and also presents an analysis on the cosmic rays detection performance of the Intermediate Tile calorimeter cells. Finally, we present a study on MonteCarlo simulations for the dilepton invariant mass in supersymetric Msugra events.

TABLE OF CONTENTS

ACKNOWLEDGEMENTS……ii

ABSTRACT……iii

LIST OF ILLUSTRATIONS……vii

LIST OF TABLES……ix

Chapter Page

1. THE ATLAS EXPERIMENT AT LCH 1

1.1 The Large Hadron Collider 1

1.2 The ATLAS Detector Overview 4

1.3 The Inner Detector 7

1.3.1 The Pixel Detector 8

1.3.2 The Semiconductor Tracker 8

1.3.3 The Transition Radiation Tracker 8

1.4 The Calorimeter System 9

1.4.1 The EM Liquid Argon Calorimeter 10

1.4.2 The Hadronic Calorimeter system 12

1.4.3 The Tile Calorimeter 13

1.4.3.1 The Barrels 13

1.4.3.2 The Modules 15

1.4.3.3 The Scintillating Tiles and fibers 17

1.4.3.4 The Girders, Fingers and Drawers 19

1.4.3.5 The Intermediate Tile Calorimeter 21

1.5 The Magnet System 22

1.6 The Muon System 23
2. ATLAS PHYSICS 25
2.1 The Standard Model 25
2.2 Higgs Physics 29
2.3 Supersymmetry 33
2.3.1 The MSSM 35
2.3.2 mSugra 36
3. COMMISIONNING AT THE TILE CALORIMETER 38
3.1 Component Description 38
3.1.1 The Low Voltage Power Supplies (LVPS) 38
3.1.2 LVPS Bricks 39
3.2 The Online Status (TOS) and the Long Run Databases 41
3.3 The Data collecting process 44
3.4 Results 47
4. M5/M7 COSMIC STUDIES FOR THE ITC 50
4.1 The ITC Cells 50
4.2 The M5/M7 datasets 51
4.3 Cosmic Analysis with M5 Dataset 57
4.3.1 Position and Energy 57
4.3.2 Detecting cosmic events in ITC cells 58
4.3.3 M5 Results 62
4.4 Cosmic Analysis with M7 Dataset 64
4.4.1 First Muon Tracks 64
4.4.2 M7 Results 67
5. DILEPTON INVARIANT MASS DISTRIBUTION IN SUSY SIMULATION 73
5.1 Experimental Signatures 73

5.2 Data Analysis 74
5.3 Results 77
6. Conclusions 81
REFERENCES……..83
BIOGRAPHICAL INFORMATION……...85

LIST OF ILLUSTRATIONS

Figure		Page
1.1	Overall view of the LHC experiments	2
1.2	LHC Dipole: standard cross-section	4
1.3	The ATLAS detector systems.	5
1.4	A Slice lateral cut of the ATLAS detector.	6
1.5	The Inner detector.	7
1.6	The calorimeter system η coverage.	10
1.7	The LAr EM calorimeter layout.	11
1.8	The Tile Calorimeter and its cells.	14
1.9	The Tile Calorimeter front view module design.	15
1.10	The sub-module design.	17
1.11	The fiber double readout system going into the PMT's	18
1.12	The cell segmentation of a Long barrel module before placing the fibers.	19
1.13	A super drawer being installed inside the module's girder.	20
1.14	The ITC sub module design.	21
1.15	The ATLAS Magnetic system	22
1.16	The ATLAS muon Spectrometer system.	23
2.1	The standard model fundamental blocks	26
2.2	Loop diagrams:(a) fermion loop, (b) gauge boson loop, (c) scalar loop.	30
2.3	Parton-Parton interaction.	31
2.4	Sensitivity for the discovery of a Higgs boson.	33
2.5	The standard model and SUSY particles.	34

3.1 Low Voltage Power Supply (LVPS) 39
3.2 Two different bricks at EBA. (a) a stable brick (b) an unstable brick. 40
3.3 Example of a TOS webpage for April 2007 Module 46 EBA partition 42
3.4 First 15 Modules of the +3VDigitizer brick from April to May (2007). 44
3.5 Summary of “TOS” classification for Mother Boards. 48
3.6 Total of 5VMB bricks of Long Run category 48
4.1 A quarter sector of Atlas Tile calorimeter. 50
4.2 A 2D histogram eta vs module for energy towers 57
4.3 Associated Cells are shown with the same color 59
4.4 EBC (D5+D4) Average energy for all modules on a Log scale (MeV) 60
4.5 EBC (D4+D5) Average energy for all modules on a Log scale (MeV) 61
4.6 Cosmic ray detection by the D4D5 (a) and the D5D4 (b) pair cells 63
4.7 Energy signal vs. module for D4D5 (a), and D5D4 (b) cell pairs 64
4.8 Some muon tracks in the tile calorimeter 65
4.9 Muon track distributions. (a) x vs. z crossing points. (b) phi vs. theta tracks 66
4.10 Response to cosmic ray, exponential + Landau fit. 68
4.11 D4, D5 and C10 cell response to cosmic muons for 4 adjacent top modules. 69
4.12 ITC cells energy distribution 70
4.13 Phi Vs. Theta distribution of muons tracks in D5 module 72
5.1 The simplest Msugra decay chain 73
5.2 lepton signals for e+e- (blue), μ+μ- (black) and e+/-μ-/+ (red) 76
5.3 Dilepton invariant mass after flavor subtraction. 77
5.4 Reconstructed d signals for for e+e- (left), μ+μ- (center) and e+/-μ-/+ (right). 78
5.5 Truth signals for for e+e- (left), μ+μ- (center) and e+/-μ-/+ (right). 79
5.6 Flavor subtraction with the new data 79

LIST OF TABLES

Table Page

1.1 The Inner detector parameters. 9

1.2 Parameters of the ATLAS calorimeter systems. 13

1.3 The ITC components. 21

2.1 The standard model of particle physics. 28

2.2 MSSM list of particles. 36

2.3 mSugra free parameters. 36

3.1 Different brick categories for the Long Run database. 43

3.2 EBA partition results for the summation of all bad categories. 45

3.3 LBC partition results for the summation of all bad categories. 47

4.1 Important M7/M5 variables inside the Ntuples. 53

4.2 DetCellTile 20 bit binary code for cells in TileCal. 54

4.3 Energy deposition for different cells. 56

4.4 Eta values on some cells. 58

4.5 Plot description. 62

4.6 Energy contribution to the muon track 71

5.1 Msugra at point 5 parameters. 75

CHAPTER 1

THE ATLAS EXPERIMENT AT LCH

The Large Hadron Collider (LHC) is a proton-proton (p-p) particle accelerator with a maximum energy of 14 TeV. The LHC is at least 7 times more powerful than any other particle accelerator ever built. Its goal is to provide experimental evidence of new physics at the TeV energy scale, in particular the existence of the Standard Model (SM) Higgs boson and experimental support for Supersymmetry (SUSY) theories. The LHC is home of 4 major experiments: CMS, LHCb, Alice, and ATLAS. In this chapter we will describe the LHC and its experiments and its detectors, but special attention will be given to the ATLAS detector because it is where the UTA high energy group is involved.

1.1 The Large Hadron Collider

The LHC (Large Hadron Collider) located at CERN, close to the city of Geneva, under the France-Switzerland border, is a subterranean ring shaped tunnel with a 27 km circumference and a 4.2 km radius. The tunnel hole by itself is 3.8 m. in diameter (an average school bus would be able to fit), and it is buried at 50 to 175 m (depending on location) below ground level (see Figure 1.1). The tunnel was constructed in the 80's as home of the LEP (Large Electron Positron Collider). This collider was at its time the most powerful collider with an energy of 208 Gev. Later, in 1989, the CERN Council approved and started the construction of the LHC using the pre-existing tunnel and removing LEP magnets. After almost 10 years of continuous work and at least 3 billion dollars in cost, the LHC is scheduled to start operation in late 2009.

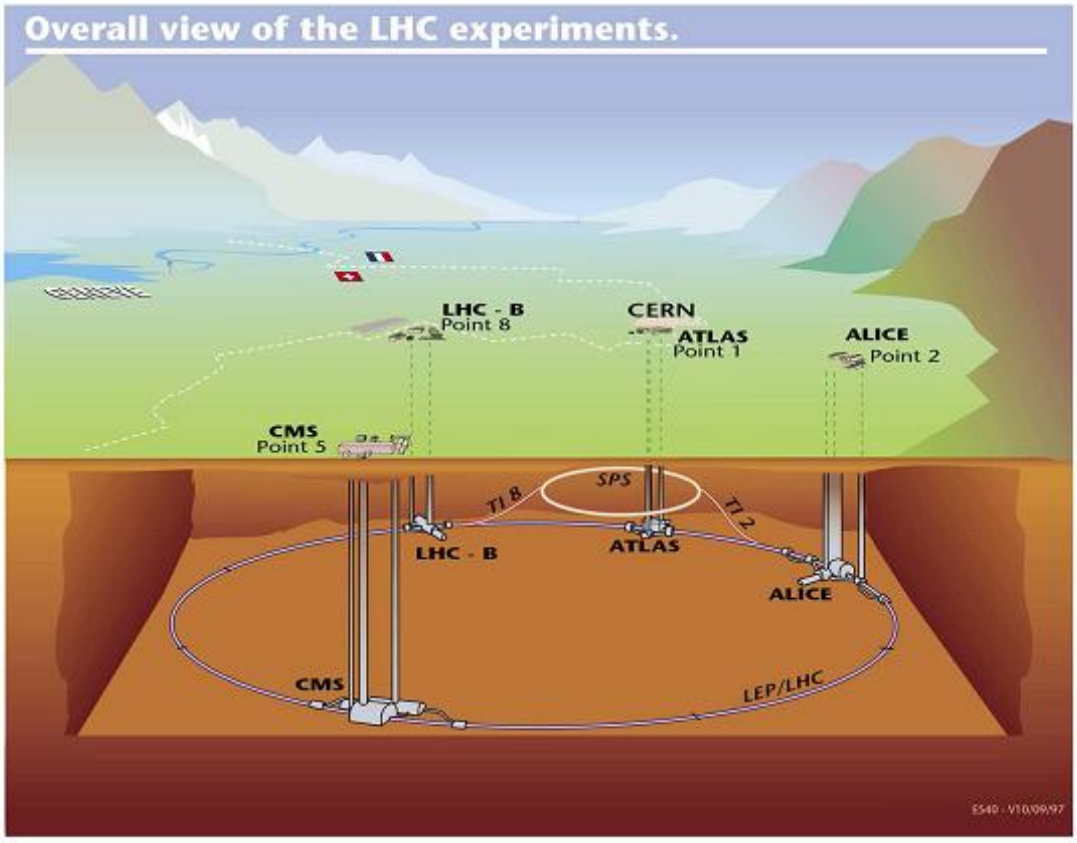

Figure 1.1 Overall view of the LHC experiments.

The LHC is a Proton-proton machine; each of the proton beams will contribute one half (7 TeV) of the total LHC energy. Nevertheless, this energy is constrained to other different variables. For example, the fact that the protons are traveling in bunches, or groups, means that there is not a continuous current of protons at all times. Therefore, to increase the number of events that are available for finding interesting physics during collisions, the luminosity factor needs to be maximized; equation 1,1 shows this relationship:

$$L = \frac{N^2 f}{4 \Pi t A_T} \tag{1.1}$$

L stands for the luminosity, N is the number of protons per bunch, f is a function that depends on the actual number of protons in the bunch that will collide, t is time between bunches and A_T is the sectional area of each bunch. For the LHC the time between bunches is approximately 25 ns; it was designed like this to ensure that after a collision all of the particles created will leave the detector before the next collision. The value of luminosity then will depend finally on the number of protons per bunch because the other variables are fixed. The luminosity will be around $10^{31}cm^{-2}s^{-1}$ for the first year of running. After that, if everything goes all right, small increases in luminosity will be done until reach the nominal luminosity value of $10^{33}cm^{-2}s^{-1}$. The number of bunches circulating the LHC at any given time is calculated to be around 2835, each bunch carrying more than 10^{11} protons.

The LCH needs two different pipes for each proton beam. This is a major difference from previous synchrotron particle-antiparticle accelerators, such as LEP at CERN and the Tevatron at Fermilab, where only one ring of magnets can hold, accelerate and conduct proton-antiproton beams. Because they are opposite in charge, they travel in opposite directions inside the same ring. Although having and extra beam pipe increases construction cost, the new design is overall an advantage because it will highly raise the luminosity (increasing the collision rate). Most importantly, it will get rid of the difficult process of creation and storage of antimatter. The LHC tunnel has 1232 superconducting dipole magnets; all of them make use of a brand new technology that accelerates the proton beams in opposite directions.

Figure 1.2 shows the standard cross section of the LHC dipole magnets that surround the two proton beams inside the LHC tunnel. We can easily see in green the two parallel proton beam pipes that are back to back to each other and transport the protons. In total we have 1292 dipole magnets working at a temperature of 1.9 Kelvin degrees. The magnets material is copper-clad

niobium-titanium. In addition to the dipole magnets, 392 quadrupole magnets are used for focusing the beams just before the collision points.

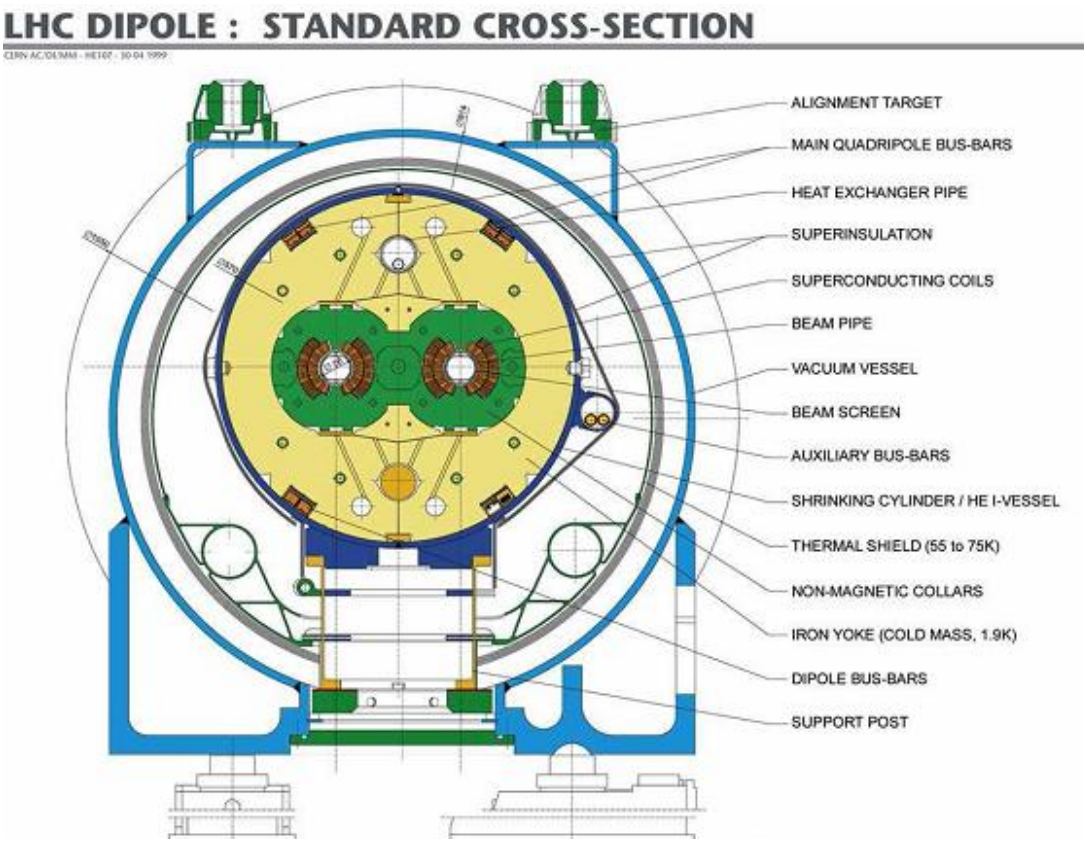

Figure 1.2 LHC Dipole: standard cross-section.

1.2 The ATLAS Detector Overview

A Toroidal LHC Apparatus (ATLAS) is the largest of all the LHC detectors. Its shape is cylindrical with a length of 44 m and it is 22 m in diameter; these are the dimensions of a typical 4 floor building. Its weight is around 7000 Tons. ATLAS is the LHC experiment closest to the CERN main site at Meyrin, and is located inside a cavern 140 m underground. It is the only LHC experiment located in Swiss territory. More than 2000 scientists work for the ATLAS collaboration,

involving more than 170 institutions from all around the world. The ATLAS detector is a multipurpose detector and it will explore the full potential of the LHC proton-proton collisions. A few examples are: the origin of the mass at the electroweak scale, the compositeness of the fundamental fermions, the investigation of CP violation in B-decays, and the detailed study of the top quark. Figure 1.3, shows a transverse cut of the ATLAS detector that reveals the different subsystems and the vast complexity that allow them to detect almost every single particle created in the high energy collisions. All of these subsystems have a specialized function. For example, the magnet system bends charged particles for momentum measurements, the inner detector measures the momentum of each charged particle, the calorimeter system measures the energies carried by the particles and finally the muon spectrometer identifies and measures all muon like particles.

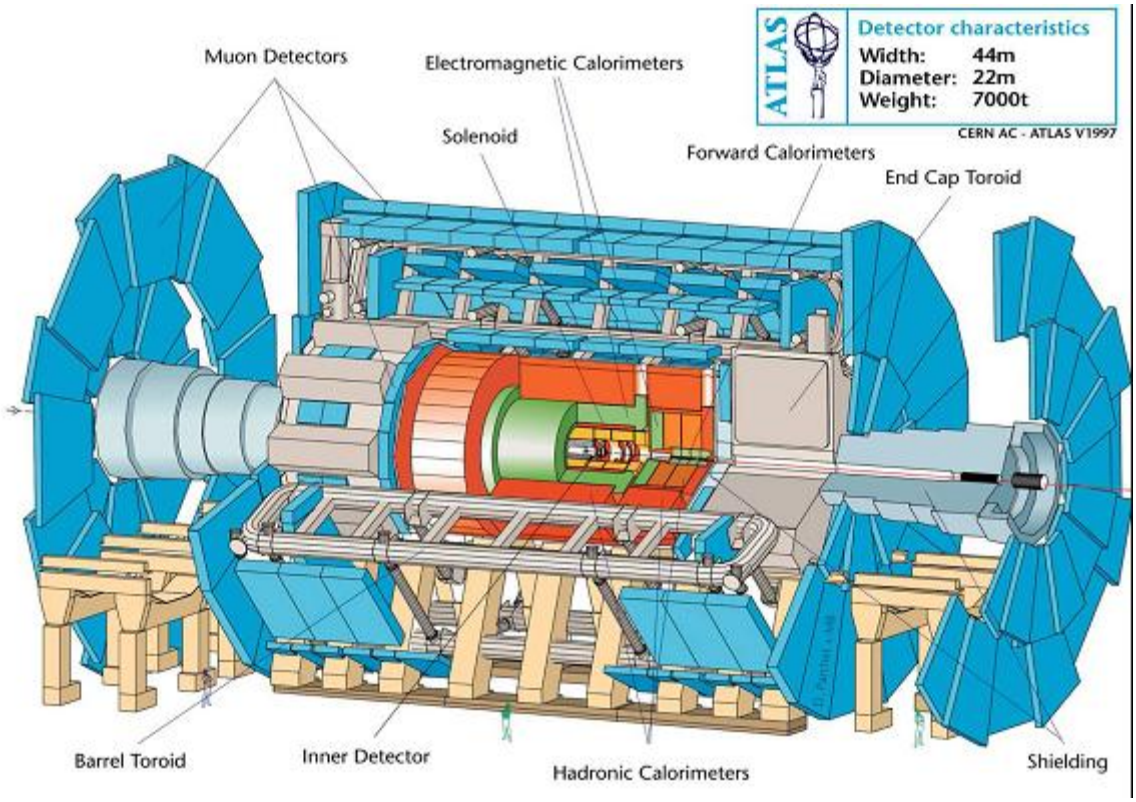

Figure 1.3 The ATLAS detector systems.

The very central part of the ATLAS detector houses the central beam pipe where the protons travel with opposite momentum and collide at the geometric center of the detector. A collision produces many other particles that travel away from the interaction point in a radial direction. The path, energy and momentum of the particles are recorded by the different sub-detectors that are shown in Figure 1.4. Most of these systems will be explained in the next sections, but special attention will be given to the Hadronic Calorimeter system. This system holds the Intermediate Tile Calorimeter (ITC) cells which are the main topic of my detector studies (Chapter 4).

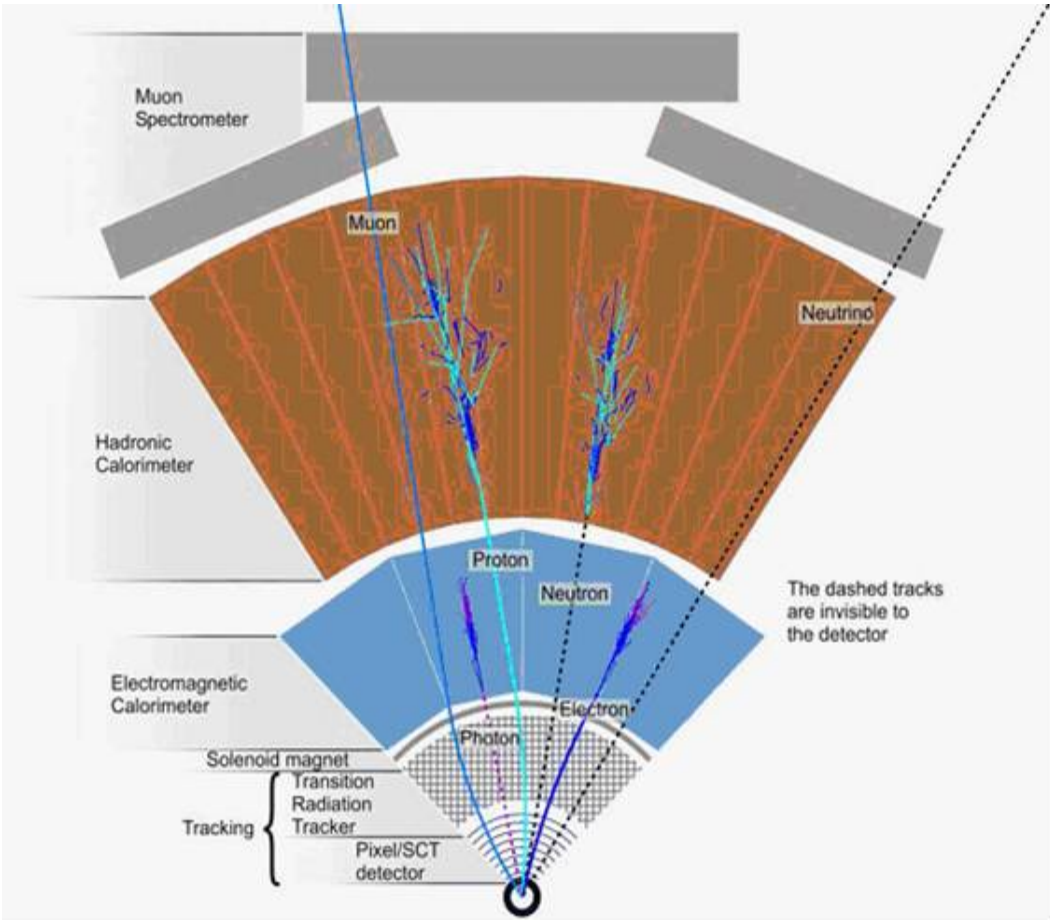

Figure 1.4 A Slice lateral cut of the ATLAS detector.

At this point it is important to introduce the concept of pseudo rapidity represented with the Greek letter "η". We will extensively use this concept in the next sections for explaining detector position. Equation 1.2 shows the relationship between η and the angle θ, measured from the XY plane:

$$\eta = -\ln\left(\tan\left(\frac{\theta}{2}\right)\right) \tag{1.2}$$

1.3 The Inner Detector

The inner detector is the innermost layer in ATLAS and also the closest one to the interaction point. It is located surrounding the beam pipe. It extends in the radial direction from a distance of almost zero up to 1.2 m and extends 4.5 m each way from the collision point for a total length of 7 m. It is designed to reconstruct tracks and decay vertices in any event with high efficiency. It also helps with electron and muon identification purposes. The magnetic field of the Inner Detector is created by a thin 2 T super-conducting solenoid with a cylindrical inner cavity. Figure 1.5 shows the different components of the Inner detector.

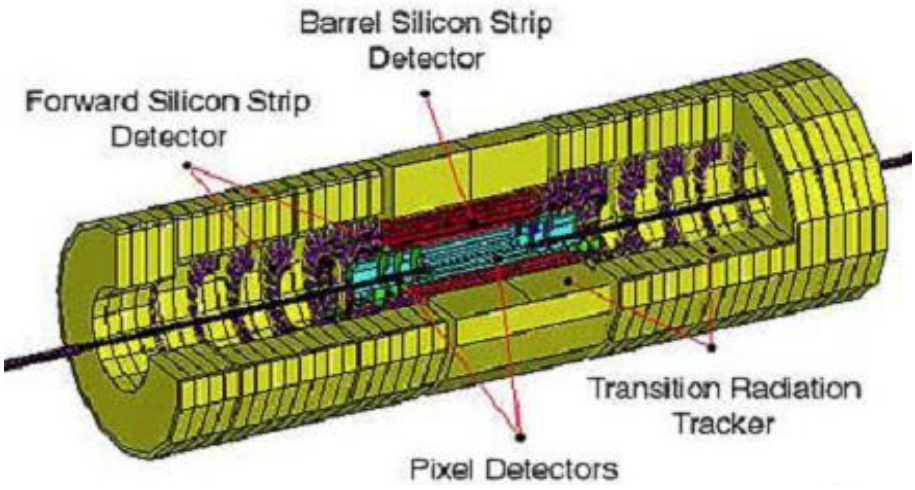

Figure 1.5 The Inner detector.

1.3.1 The Pixel Detector

The Pixel detector is a high resolution detector located as close as possible to the interaction point. It consists of three barrels at radii of 4 cm, 11 cm, and 14 cm, and four disks on each side, between radii of 11 and 20 cm. This system contains approximately 1500 identical barrel modules and 1000 identical disk modules. The read out of the pixels requires the use of advanced microprocessors because it needs to cover a large area of individual micro circuits for each pixel element. Each microprocessor must be resistant to high radiation levels.

1.3.2 The Semiconductor Tracker

The Semiconductor Tracker detector (SCT) uses silicon micro strips technology to provide high precision momentum measurements in the intermediate tracking region. The SCT also provide high granularity measurements of vertex positions needed for pattern recognition. The detector is made of eight layers of silicon material for a total area of 61 m^2. The spatial resolution is 16 μm in Rϕ and 580 μm in Z per module. This ultra high resolution requires the use of at least 5 million read out channels.

1.3.3 The Transition Radiation Tracker

The Transition Radiation Tracker (TRT) is based on the use of straw detectors of 4 mm in diameter and 1.44 m long. The barrel region of the TRT contains about 50000 of these straws while the end-caps have 320000. The total number of read out channels is 420000. The TRT is operated with X ray technology that detects ionization from the straws when a charge particle interacts with them. These straws are filled non-flammable gas mixture at 1500 V difference allowing detection by transition radiation and a large number of measurements on every track. Table 1.1 summarizes some of the detector details explained above.

Table 1.1 The Inner detector parameters.

Detector	Position and quantity	Area (m2)	Channels	η Coverage
Pixels	Removable barrel layer (1)	0.2	16 X 106	±2.5
	Barrel layers (2)	1.4	81 X 106	±1.7
	End caps disk (4 on each side)	0.7	43 X 106	±1.7 to ±2.5
SCT	Barrel layers (4)	34.4	3.2 X 106	±1.4
	End cap wheels (9 on each side)	26.7	3.0 X 106	±1.4 to ±2.5
TRT	Axial barrel Straws	--	1.0 X 105	±0.7
	Radial end cap straws	--	3.2 X 105	±0.7 to ±2.5

1.4 The Calorimeter System

The calorimeter system is in charge of accurately recording the energy deposition of the particles that leave the inner tracker. It is also responsible for interact with the calorimeter material and measure the missing transverse energy of events.

The system is divided into three main parts: one big central long barrel and two symmetric extended barrels on each end side of the detector. The central and extended barrels barrel covers the region $|Z|<2.8$ and 3.1 m $<|Z|<6.1$ m respectively. A gap region separates the main long barrel from the extended barrels. This gap region provides space for different services such cabling and cooling systems input/output. Figure 1.6 shows four different calorimeter systems, all using different technologies for different particle detection in different "η" regions. They will be described below.

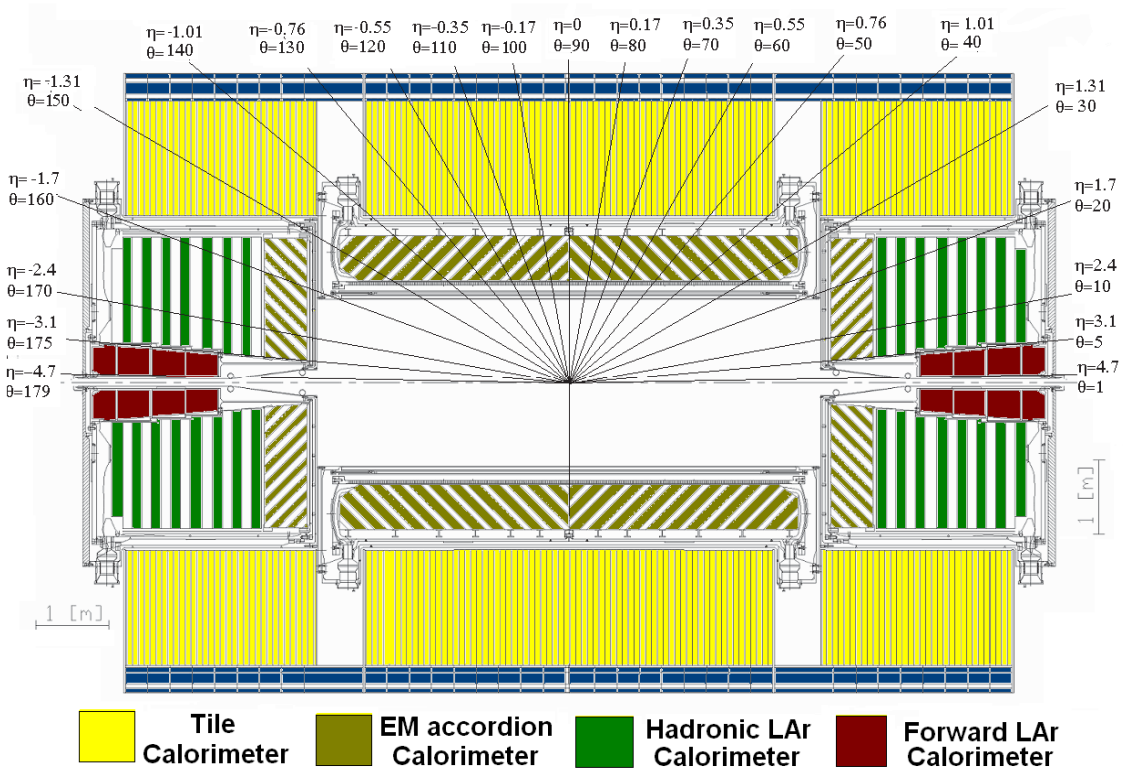

Figure 1.6 The calorimeter system η coverage.

1.4.1 The EM Liquid Argon Calorimeter

Located just outside the inner tracker, is the apparatus in charge of all measurements of electron, positron and photons deposition energies. These particles will deposit their energy and momentum when interacting with the calorimeter and at the same time they will free more electrons. The previous process is known as “electron showers”. Other charged particles, such as hadrons, also will loose energy when crossing through this second detector stage but they are energetic enough to make it into the next division, the Hadron Calorimeter.

Figure 1.7 shows a layout of the electromagnetic (EM) calorimeter. Notice the accordion shape sections to the sides which integrate the EM calorimeter. The Electromagnetic calorimeter uses liquid argon (LAr) technology with accordion shaped electrodes and lead absorber plates over it full coverage. The EM LAr calorimeter consist of two main bodies one in the main barrel covering $|\eta|<1.475$ and the other two located at the end caps in the $1.37<|\eta|<3.2$ region.

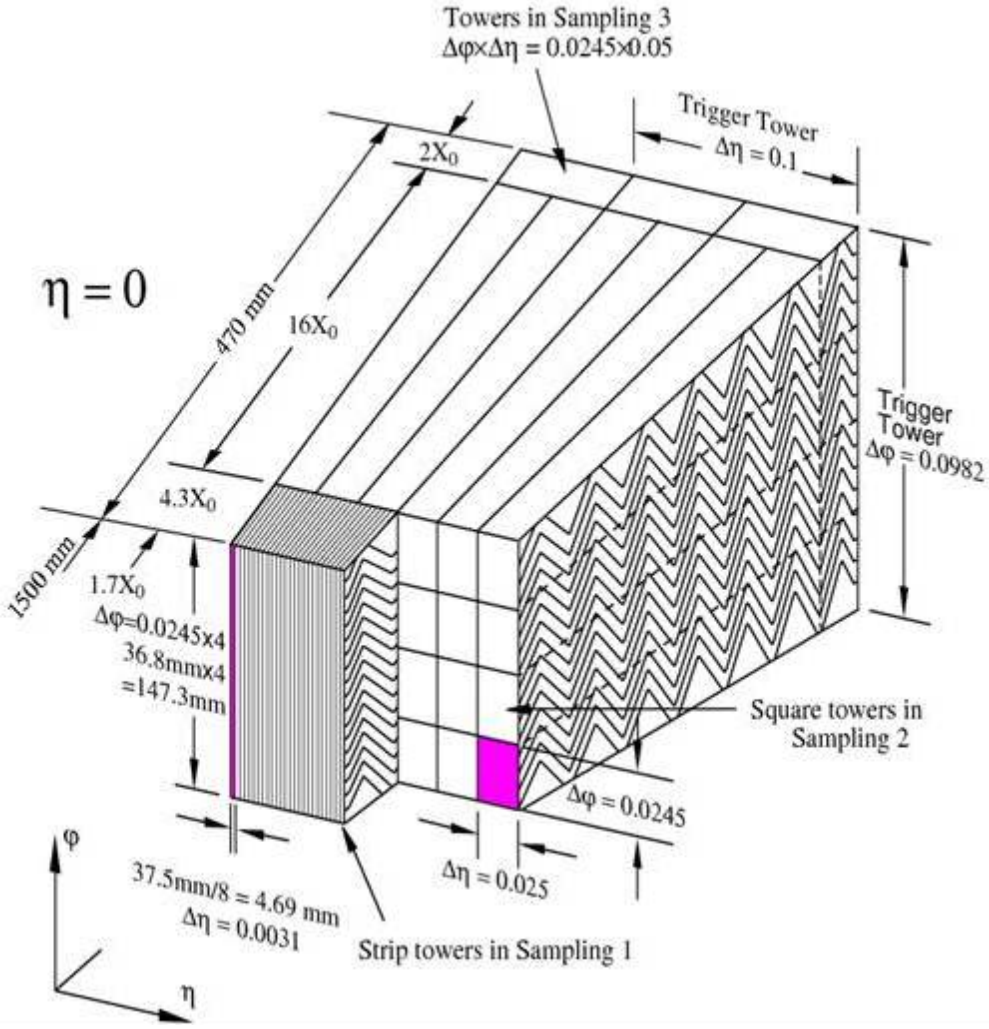

Figure 1.7 The LAr EM calorimeter layout.

The barrel calorimeter that surrounds completely the Inner tracking consist of two identical half barrels separated with a 6 mm gap region at the geometric center (Z=0). The Liquid Argon technology is used because of its excellent ability to be radiation resistant for long period of times. In addition, the LAr calorimeters have good hermeticity and good energy resolutions. The total thickness of the electromagnetic barrel and the end cap calorimeters are 24 and 26 radiation lengths respectively. The electron and photons energy losses increase at large η regions. To prevent these losses a pre sampler detector is used. The number of channels in the EM calorimeter is 200000 giving it an excellent segmentation and high resolution.

1.4.2 The Hadronic Calorimeter system

The main function of the hadronic calorimeter is the identification and measurement of the missing transverse momentum of particles in an event. This information is used primarily for jet reconstruction. The Hadronic particles interact with the detector material after leaving the EM calorimeter. The ATLAS Hadronic calorimeter system covers the pseudorapidity region, $|\eta| < 4.9$. This wide region is covered with the help of different hadronic detectors, one of each, covering different η sub-regions and using different technologies. For example over the range $|\eta| < 1.7$, the iron scintillation tile technique is used in the tile calorimeter (we dedicate a special section for describing it), while the LAr technology is used for both the forward calorimeter and the end cap calorimeter at the extended barrels. The Hadronic End Cap (HEC) calorimeter will cover the range $1.6<|\eta|<3.2$, and the forward calorimeter (FCAL) in the range $3.1<|\eta|<4.2$, both FCAL and HEC shares the same cooling system with the extended EM calorimeter. The Forward calorimeter is extremely bombarded by radiation so its design contemplates this fact. It is made of copper and tungsten with liquid Argon as the sensitive medium. The HEC consist of two wheels with a radius of 2.03 m, each of these wheels contains equally specialized concentric copper plates with a gap region between them. In the gap region special electrodes will calculate

and then transmit the information related with the hadronic energy deposition. Table 1.2 summarizes different properties from different subsystems of the Hadronic calorimeter.

Table 1.2 Parameters of the ATLAS calorimeter systems.

	EM Calorimeter	LAr HEC	LAr FCAL	Tile Calorimeter
$\|\eta\|$ coverage	0 - 3.2	1.5 – 3.2	3.1 – 4.9	0 – 1.6
Partitions	7	4	3	4
Readout channels	214000	8600	1500	10000

1.4.3 The Tile Calorimeter

The Tile calorimeter is a 2300 Ton sampling hadronic calorimeter mostly made of steel (used as the absorber medium) and plastic scintillating plates (as the active medium) for measuring the deposited hadron particle energies. The detector geometry is basically a 12.2 meters long cylinder, with a inner radius of 2280 mm and a outer radius of 4230 mm, that surrounds the EM calorimeter covering the $|\eta|<1.7$ region.

1.4.3.1 The Barrels

The Tile calorimeter is divided into three main cylinder blocks (called barrels), in the longitudinal direction, one long central barrel (LB) and two extended barrels (EB) to each side. They are separated from the central barrel by a gap region. Figure 1.8 shows a cut of the Tile calorimeter view. Because the Tile calorimeter is symmetric in the Z axis, it is convenient to divide the center long barrel into two pieces (this is an imaginary division the actual center barrel is just one piece), one to each side of the detector. We have grand total of two long (not as long any more) central barrels (EBA and EBC) and two extended barrels (EBA and EBC), where the A side is the north face of the detector (towards the Jura Mountains) and the C side is the south face (towards Geneva).

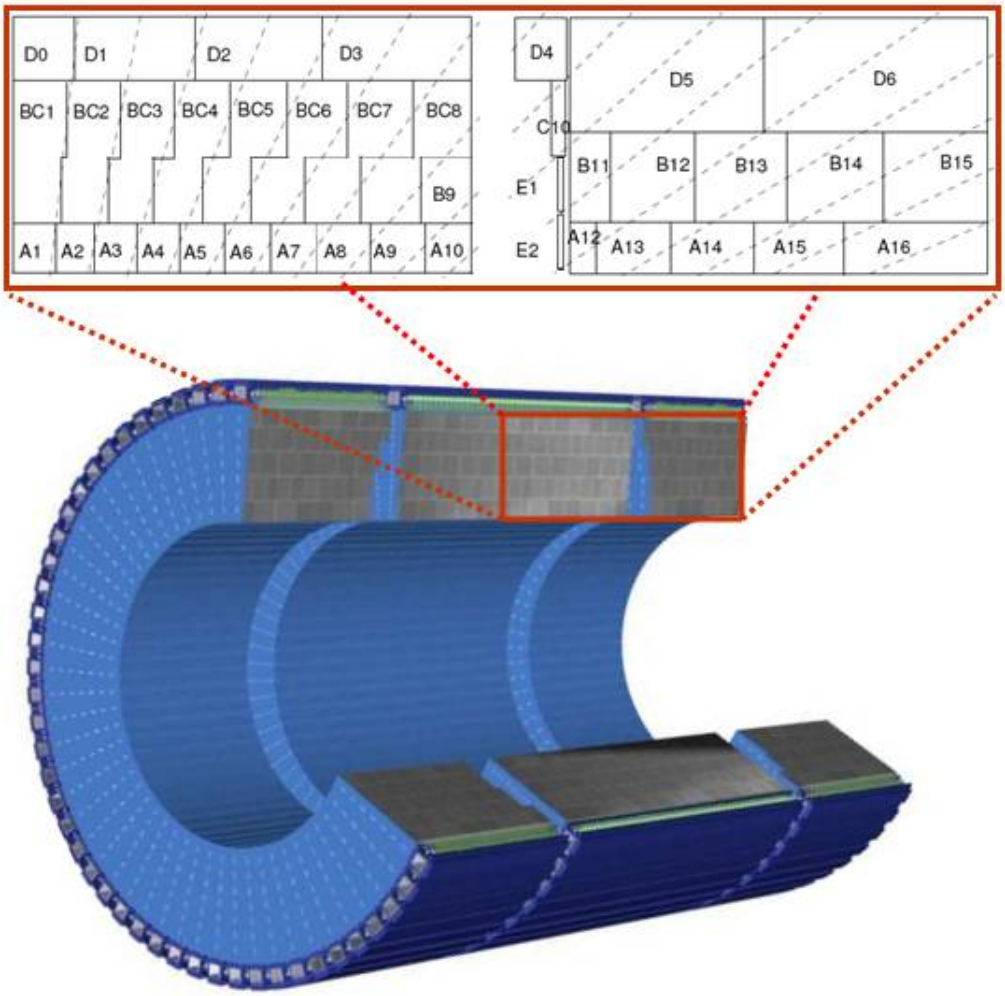

Figure 1.8 The Tile Calorimeter and its cells.

Each extended barrel is 2910 cm long and covers the $0.8<|\eta|<1.7$ region while the central barrel is 5640 cm and covers the $|\eta|<1.0$ region. The distance between the extended barrel and the main barrel is about 600 mm and it is known as the crack or gap region. In that region is located an addition to the extended barrel called the intermediate tile calorimeter; it will be explained in detail in a later section.. In addition to the longitudinal division, there is another 64 azimuthal partition; any of those blocks are called modules. Figure 1.8 also shows the two gap regions between barrels and the modules.

1.4.3.2 The Modules

The tile calorimeter was not built in one single piece. Instead it was fabricated in small segments, called modules, at different collaborating institutions and then brought together to the CERN site for later assembly to its final 100 m underground position. For example, all 64 modules from the EBA and EBC partition were built at Argonne National Laboratory in the US, and in Barcelona, Spain respectively. The ITC modules were built at the University of Texas at Arlington.

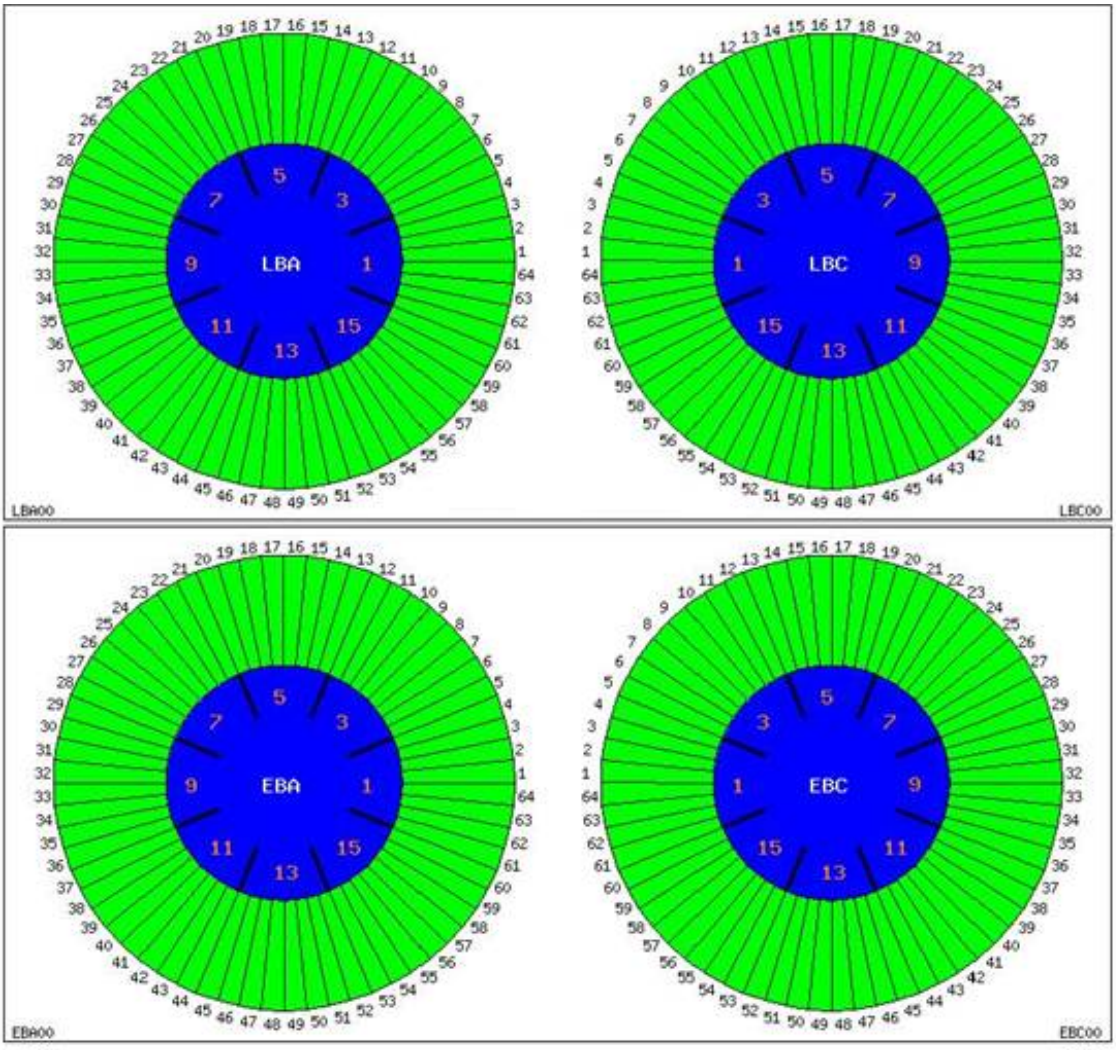

Figure 1.9 The Tile Calorimeter front view module design.

Figure 1.9 shows a front view of the four tile calorimeter partitions with the 64 modules division in light green, with the partition number on the outside of the circumference. Notice that the nomenclature depends on the partition position (module 1 will always be towards the inside of the LHC ring for all the partitions). The blue color represents other ATLAS systems such as the EM calorimeter, the inner detector etc.

All modules belonging to the same partition are completely identical in design and structure. In addition, they are functionally independent from each other, expect for the refrigeration system and some cabling communication system. The modules are held together by an external metallic skeleton that anchors to their external body structure.

The structure of all the tile calorimeter modules is a longitudinal repetition of layers of steel plates with pockets where the scintillator tiles are located in a ratio of 4 to 1. These repeated elements are known as sub-modules. Multiple sub-modules will eventually complete a module. For example, a module of the central barrel has 19 sub-modules whereas those of the extended barrels only have 10.

A sub-module is made up of 2 large 5 mm thick trapezoidal steal plates called master plates (all master plates have the same area) and 12 smaller trapezoidal plates of 4 mm thick called spacer plates (which area varies). These plate combination is called a period; once 16 periods are stacked, one over the other, they complete a sub-module. The scintillating tiles are 3 mm thick and they are located between steel spacers plates. Figure 1.10 shows the spacers in white and the master plates in gray.

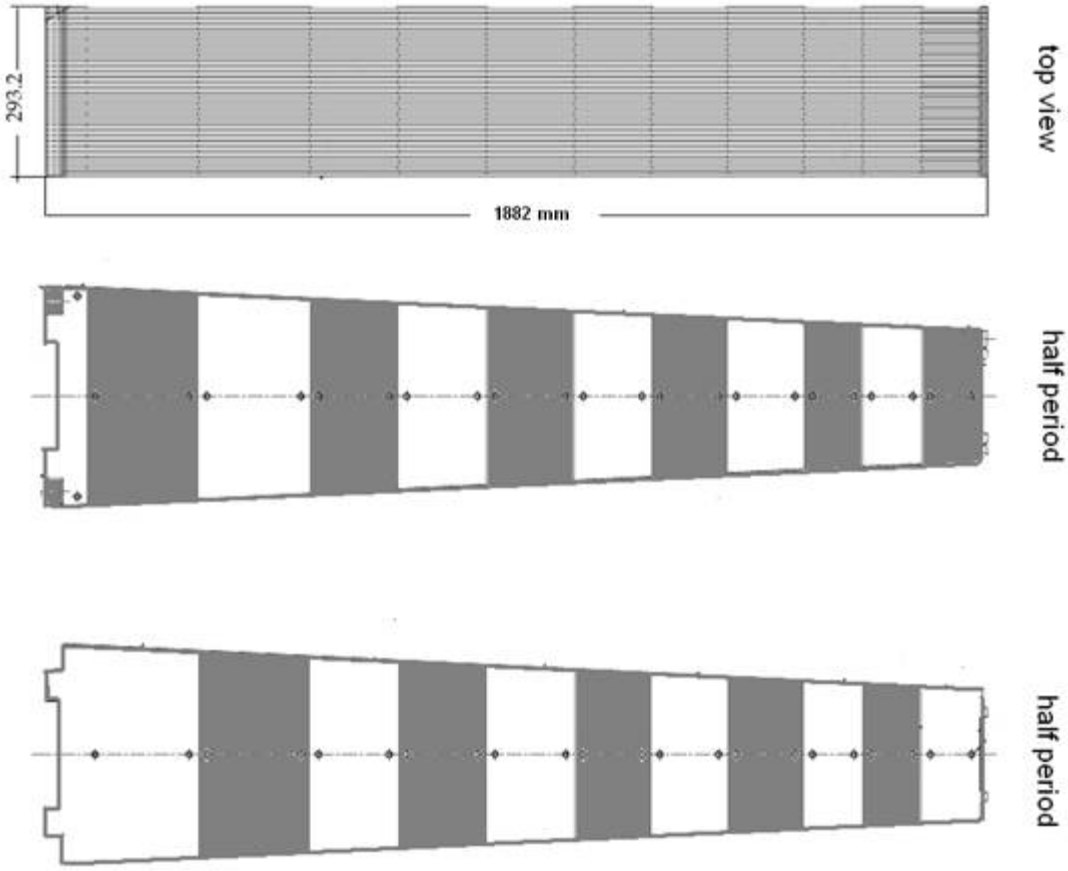

Figure 1.10 The sub-module design.

1.4.3.3 The Scintillating Tiles and fibers

After the steel plate periods are assembled, the plastic scintillating tiles are inserted into the module pockets. The light produced by particles interacting with these active materials is captured by using Wave Length Shifting (WLS) optical fibers and transmitted to the photomultipliers (PMT's). The use of WLS fibers allows the scintillating tiles to be positioned parallel to the particle trajectory. This is an innovation feature in any other calorimeter built to date. This fact in addition to make the readout easier, will allow for a double readout from both sides of the tile in the module. This type of read outs will provide redundancy to account for the

cases when one of the read outs is damaged or not working properly. Figure 1.11 shows the fiber scheme.

Figure 1.11 The fiber double readout system going into the PMT's.

The fibers are grouped in bundles at the outer end of the detector and every bundle goes to a specific PMT. This grouping defines the division of the modules into cells as shown previously in Figure 1.8. The cell division will depends on which partition the module belongs to.

Figure 1.12 shows a photograph of a long barrel module cell distribution before any fiber or electronics were assembled. The cell distribution is divided into four groups called A, B, C and D. They depend on the radial distance from the beam pipe. Cells from different groups and different

partitions have different sizes. “A” cells are normally smaller than “B” cells and so on; the D group has the largest cell sizes. A group of cells that belong to a same η region form a tower.

Figure 1.12 The cell segmentation of a Long barrel module before placing the fibers.

1.4.3.4 The Girders, Fingers and Drawers

On the outer part of the tile calorimeter and just above the D cells group, is located a hollow squared metallic structure that provides physical support for the sub-modules installation process. This structure is called the girder, and it covers the total length of a module. The girder and is connected to the other girder modules for structural support. Inside the girders is an additional removable structure of 1.5 m long called drawers. They hold the front end electronics and the 24 PMT’s. A set of two drawers is called a super drawer. They are inserted into the girder from the

gap region side of the module and this is convenient so that one super-drawer is needed to readout each module for all four barrels.

At the end of each super drawer towards the gap region side (and still as part of the girder) we found a region called the finger. They are the final piece of a module and they house the powers supplies that will feed voltages to the PMT's and to the electronics system. Figure 1.13 shows a super drawer being inserted inside a module during a test beam in 1999. The same principle applies for the already installed modules at the ATLAS cavern if it is necessary to remove a super drawer for repair.

Figure 1.13 A super drawer being installed inside the module's girder.

1.4.3.5 The Intermediate Tile Calorimeter

The Intermediate Tile Calorimeter, or ITC, is a special sub-module in the 680 mm gap region. It still belongs to the extended barrel partition although it is installed after the 64 modules of the external barrel are assembled. It covers the $0.8<|\eta|<1.6$ region. The structure of the ITC depends of the η region where it is located as depicted in Table 1.3.

Table 1.3 The ITC components.

ITC η Region	ITC name	Material	N of Cells
0.8 - 0.9	Plug	311 mm steel + scintillator stack	1
0.9 - 1.0	Plug	96 mm steel + scintillator stack	1
1.0 - 1.2	Gap scintillators	Scintillators only	2
1.2 - 1.6	Crack scintillators	Scintillators only	2

Figure 1.14 shows the ITC period structure and dimensions for one module. We can identify the plug region from 0 to 911 mm where we find cells D4 and C10 (see also Picture 1.12) and the gap region from 912 to 1602 mm containing cells E1 to E2. The Crack region contains cells D3 and D4 and is not shown in the picture.

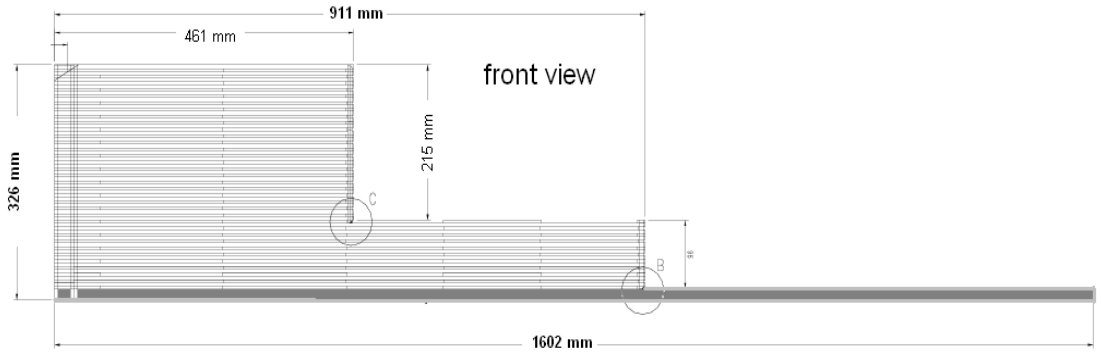

Figure 1.14 The ITC sub module design.

1.5 The Magnet System

The ATLAS detector's magnetic system provides a strong magnetic field able to bend the charge particle trajectories in order to accurately measure their respective momenta. It is divided into a Central Solenoid (CS), providing an axial magnetic field for the inner tracker, and three large air-core toroids, with a tangential magnetic field for the muon spectrometer. Figure 1.15 shows a scheme of the magnet system.

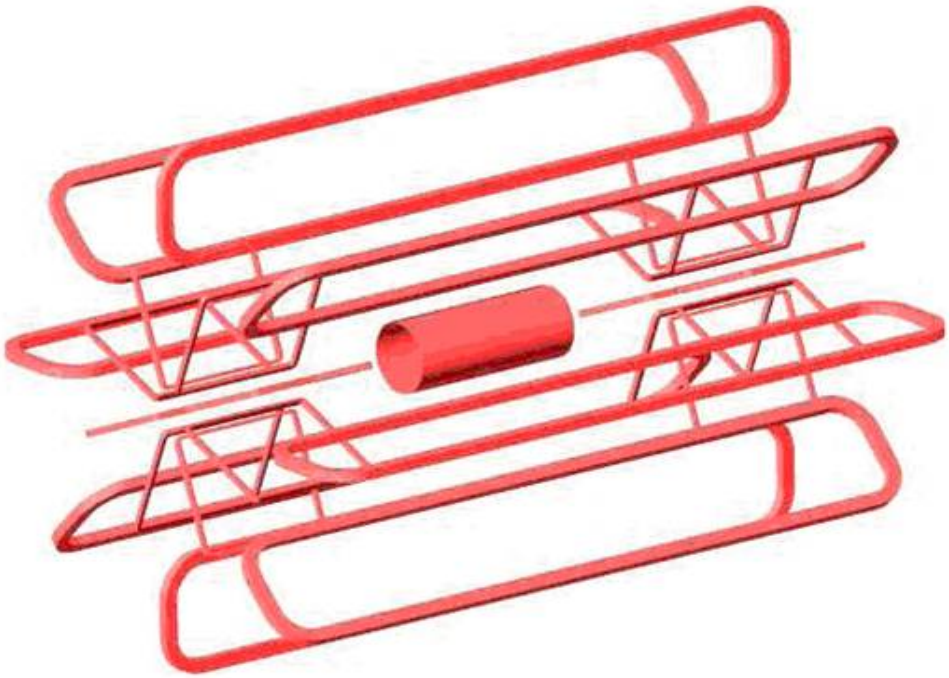

Figure 1.15 The ATLAS Magnetic system.

The Central Solenoid is made as a single layer coil and provides a strong magnetic field (about 2 Tesla). The CS is a conduction-cooled superconducting solenoid based on a thin-walled construction for minimum thickness to decrease particle scattering effects. The air core toroid magnet system consists of one central Barrel Toroids (BT) and 2 End-Cap Toroids (ECT). Each of the toroids is a made up of eight flat aluminum coil magnets. The BT dimensions are 25 m long and 5 m wide. It generates the magnetic field for the central region of the muon detector. The

ECT dimensions are 5.6 m long and 1.2 m wide. In summary, the magnet system is 25 meters long and 20 meters in diameter and with a total weight of 1300 tons, cooled by liquid helium at 4.8 K. The magnet system stores a magnetic energy close to 1600 MJ.

1.6 The Muon System

The muon Spectrometer is the last detector layer of ATLAS detector. It is located surrounding the tile calorimeter, and extends from a radius of 2.5 m to a radius of 11 m. it is based on a modular design with total area of 12,000 m2. Figure 1.16 shows the different chambers of the muon detector system inside the ATLAS detector.

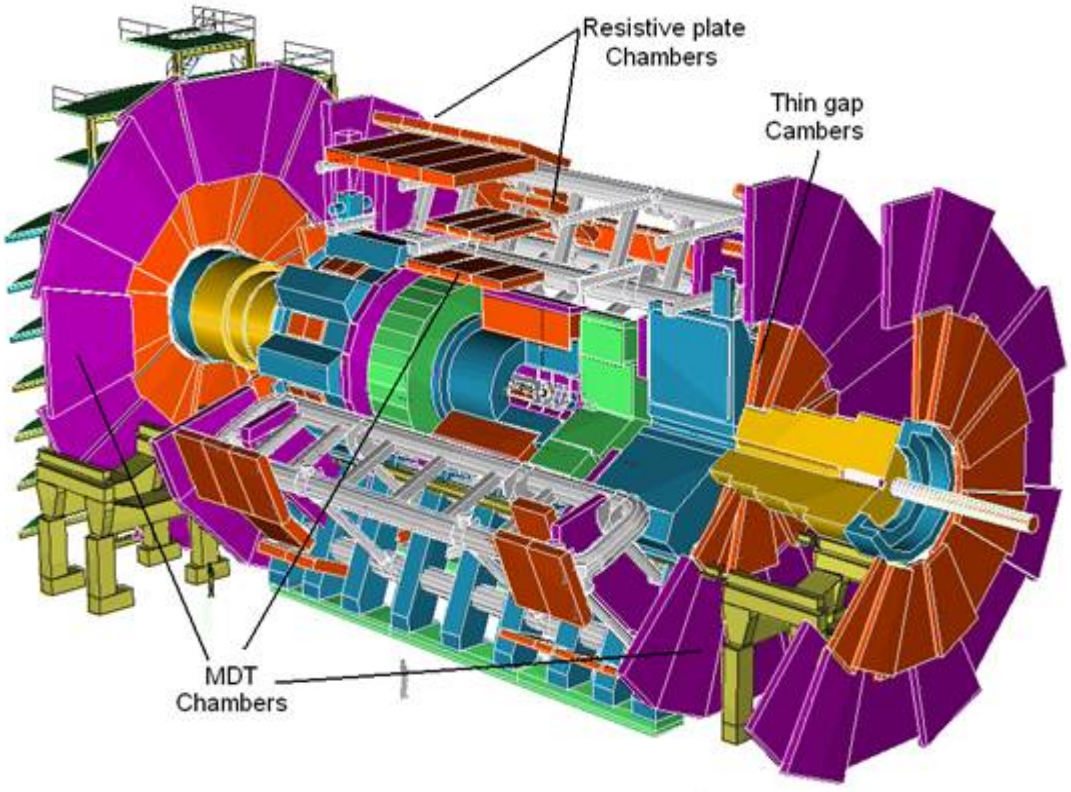

Figure 1.16 The ATLAS muon Spectrometer system.

The ATLAS muon Spectrometer is based on the deflection of the muon particles tracks due to the magnetic field provided by the super-conducting air-core toroid magnets. Momentum measurements are done by the Monitored Drift Tubes (MDT) with a trigger provided by the Resistive Plate Chambers (RPC). In regions with large η Cathode Strip Chambers (CSCs) are employed and its trigger signal is supplied by the Thin Gas Chambers (TGC). In the barrel, the chambers are arranged in three concentric cylinders that surround the θ region completely. The end caps are arranged in four disks one located just after the other. This arrangement guarantee that muon particles coming from the interaction point traverse at least three chambers regardless of their "η". There are around one million channels in this muon detection system.

CHAPTER 2

ATLAS PHYSICS

The first proton-proton collisions at the LHC are schedule to begin in late 2009. After that date, we hope to find experimental confirmation of the existence of new physics beyond the standard model, in the never before explored TeV region. Theoretical physicists have developed different theories that attempt to explain some of the most compelling questions of the natural world. Examples of these questions are: why the regular matter that composes planets and galaxies accounts only for 5% of the total universe? Why are the proportions of matter and antimatter in the universe so extremely different? What is the mechanism that gives elementary particles different values of mass? Once the LHC's experimental data is available, we will be able to analyze it and determine if the theories of the Higgs mechanism, CP violation or Supersymmetry are the laws chosen by nature.

2.1 The Standard Model

The Standard Model (SM), to date, is our best description of the components of matter. It describes the fundamental composition of atoms, molecules, human beings and all the things we know. The SM was developed during the second half of the 20^{th} century based on quantum field theory which quantizes the electromagnetic, the weak and the strong forces into spin 1 particles called bosons, carriers of the forces, and ½ spin particles, called fermions. The number of bosons and fermions is limited to 25. They are: 12 fermions, 12 bosons and an additional not yet discovered Higgs boson. Figure 2.1 shows a summary of the particles explained before.

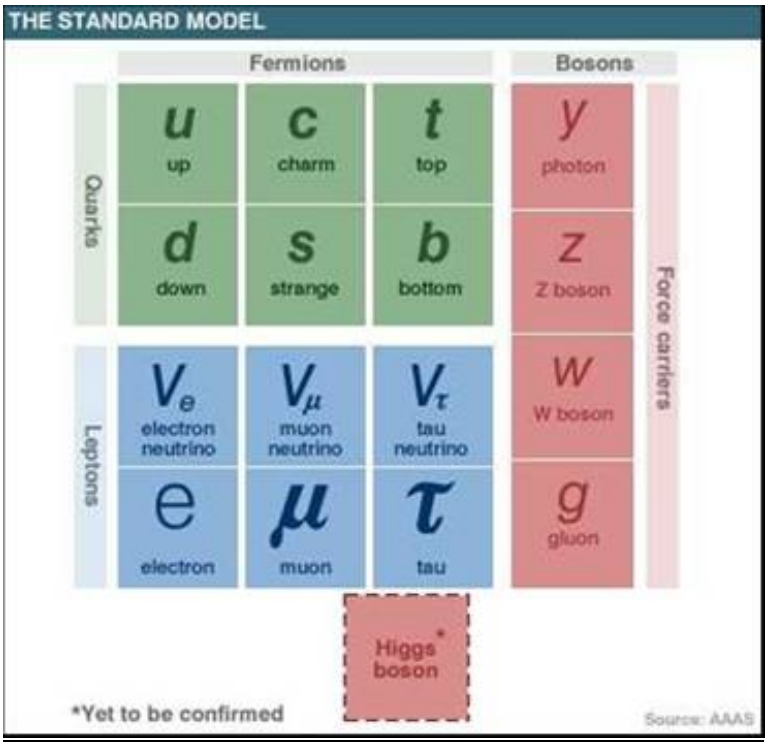

Figure 2.1 The standard model fundamental blocks.

Quarks, leptons and bosons are the building blocks that constitute all the matter we are familiar with. In addition these particles apparently have no internal structure, thus they are fundamental and indivisible. Quarks associate with other quarks and gluons to form sub-atomic particles called hadrons. Hadrons are classified into two categories, mesons and baryons formed by two and three quarks respectively. Two mesons examples are the pion, formed by $u\bar{d}$ quark pair (the bar means the antiparticle) and the kaon $s\bar{d}$. Baryons examples are the familiar proton uud and neutron udd . Quarks are not found in an isolation state (known as quark confinement).

Interactions between quarks are mediated by the strong force, so they carry an additional charge know as color. This charge comes in three kinds (or colors): red, blue, and green. The strong force is carried by eight vector gluon bosons, which carry no electric charge, only color charge.

Quarks also can interact via the electromagnetic force where the massless and neutral photon is the force carrier plus the weak force and its massive triplet boson carrier (W+, W- and Z_0). On the other hand, leptons do not feel the strong force. They interact either weakly or electromagnetically. The electron, muon and tau are completely identical except for their masses. They all carry an electromagnetic charge of one, while all neutrinos are electrically neutral and almost massless.

The standard model introduces the concept of generations of quarks and leptons. Figure 2.1 shows same particle generations in the same column. For example the first generation quarks are the up (u) and the down (n) quarks while the first lepton generation particles are the electron (e) and the electron neutrino (Ve), the second quark generation consist of the strange (s) and charm (c) quarks, and the second lepton generation are the muon and muon neutrino. Finally top and bottom quarks form the third quark generation and the tau and its neutrino complete it for the leptons. A notable relationship between members of the same generation is that they present a difference of ±1 in electric charge. Finally for having a complete description of the SM we should add to Figure 2.1 another set of particle which are an exact replica of the particles above, except for the values of electric charge, which is opposite. These particles are known as antimatter and they play a crucial role in the success of the SM.

We are excluding the SM Higgs boson for now, because it is still a theoretical SM particle, nevertheless we will dedicate an entire section to its description. We will also provide an explanation on the different techniques that there will be use at the ATLAS detector for the Higgs search. Table 2.1 classifies the standard model particles and shows the different mass values for all of them.

Table 2.1 The standard model of particle physics.

FERMIONS matter constituents, half odd integer spin						BOSONS: force carriers, integer spin		
Leptons spin 1/2			Quarks spin 1/2					
Flavor	Mass GeV/C^2	Electric charge	Flavor	Mass GeV/C^2	Electric charge	Flavor	Mass GeV/C^2	Electric charge
ν_e electron neutrino	< 0.2 X 10^{-9}	0	**u** up	0.002	2/3	γ photon	0	0
e electron	0.000511	-1	**d** down	0.005	-1/3	W^- W boson	80.39	-1
ν_μ muon neutrino	< 0.0002	0	**c** charm	1.3	2/3	W^+ W boson	80.39	+1
μ muon	0.106	-1	**s** strange	0.1	-1/3	Z^0 Z boson	91.188	0
ν_τ tau neutrino	< 0.0015	0	**t** top	173	2/3	**g** gluon	0	0
τ tau	1.777	-1	**b** bottom	4.2	-1/3	**H** Higgs boson	undiscovered	

The standard model's beauty arises from its perfect connection between gauge theory and the pure mathematical description of group theory. We can connect one of the three different forces with a mathematical group and its force carriers with the generators of that particular mathematical group. The electromagnetic force is perfectly described in terms of the one dimensional unitary group U(1). This group, mathematically speaking, defines rotation of complex numbers with unitary magnitude in one dimension. And it is directly related to cartisian vector rotations in 2 dimensions, so it only has one generator (rotations of a θ angle). This means that the electromagnetic force will have only one carrier, the photon.

The SU(2) group entirely describes the weak interaction between particles. SU(2) is the special unitary group of rotations of complex numbers in 2 dimensions. It is interesting that its morphology is similar to vector rotations in 3 dimensions. For example it has 3 generators, one for each dimension, and matches the three force carriers W+, W- and Z.

The group SU(3), rotation of complex numbers in 3 dimensions has no representation in cartisian algebra, but we know this group represents the strong force and it has 8 generators, again, It matches the number of carries of the strong force (8 gluons in the SM). In the SM, the SU(2) X U(1) symmetry groups are combined to describe the electroweak theory. This electroweak interaction can be spontaneously broken if we postulate the existence of a Higgs field and a Higgs particle. This particle will provide mass to vector bosons, W and Z which mediate the weak interaction, but not to the electromagnetic force carrier, the photon.

The prediction power of the standard model theory during the last 30 years of discoveries in particle physics has been very successful. However it is not a complete theory and it needs at least 17 input parameters to work. Among these parameters are the three lepton and the six quark masses, the mass of the Z boson and the parameters describing the mixing quarks eigenstates of the (CKM matrix).

2.2 Higgs Physics

The electroweak sector of the standard model is described by the gauge theory. In its basic form it describes all the electroweak interactions between fermions by the exchange of massless vector bosons. If one try to Introduce the concept of mass in the SU(2) x U(1) frame, one will find that the Lagrangian will be no longer be invariant under the U(1) or SU(2) gauge transformation. One way to fix the problem is by introducing the concept of spontaneous symmetry breaking in order to give masses to the W and Z. This concept also keep the SU(2) x U(1) invariant, and it is possible to introduce a higgs mechanism to provide masses to the all SM particles.

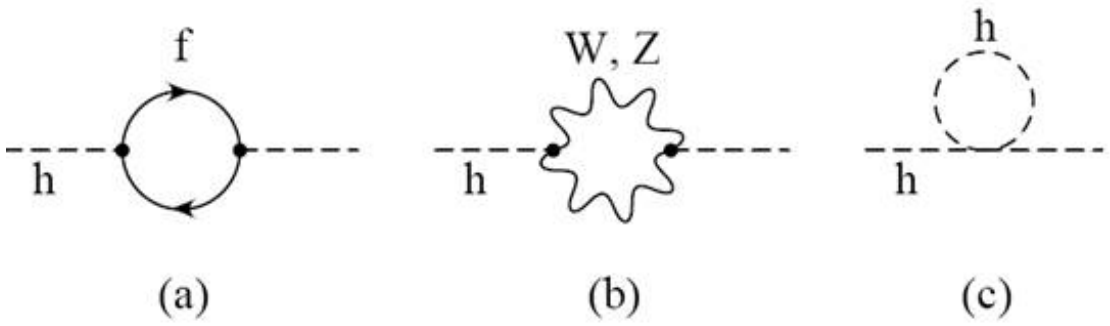

Figure 2.2 Loop diagrams:(a) fermion loop, (b) gauge boson loop, (c) scalar loop.

Nevertheless the SM by itself will not provide an ultimate mass value for the Higgs particle, but rather will introduce a new conflict in the theory called the Hierarchy problem. This problem arises because there are large corrections to the higgs bare mass due to loop diagrams as the one shown in Figure 2.2. These loop corrections need to be added forcing the higgs mass to grow quadratically with the cut-off scale and consequently to diverge as in Equation 2.1.

$$m_H^2 = m_0^2 + \delta m_H^2 \tag{2.1}$$

For a fermion loop with mass mf and a coupling □f to the higgs field we have a contribution to the square of the mass via a diagram such as in Figure 2.2 (a).

$$\delta M_H^2 = \frac{|\lambda_f|^2}{16\pi^2}\left(-2\Lambda^2 + 6m_f^2 \ln\left(\frac{\Lambda}{m_f}\right) + \ldots\right) \tag{2.2}$$

For a scalar loop like in figure 2.2(c) mass m_s and a coupling λ_s to the higgs field there is a similar correction.

$$\delta M_H^2 = \frac{|\lambda_f|^2}{16\pi^2}\left(\Lambda^2 - 2m_s^2 \ln\left(\frac{\Lambda}{m_s}\right) + \ldots\right) \tag{2.3}$$

Λ is the energy scale at with interactions not included in the SM become significant (cut-off scale).

The methods that will be used in the search for the SM Higgs boson at the LHC, and specifically with the ATLAS detector, will be determined by the selection of a specific Higgs decay channel. For example, at the LCH, Protons with same magnitude but opposite momentum will collide head to head producing a series of reactions where new particles will be created. One of those particles can be the higgs boson which eventually will decay into many more different particles. The different ways in which this decay can happen are known as channels. The calculation of the probabilities that any of these specific channels will occur is known as a branching ratio. Unfortunately, branching radios for the Higgs particle are extremely difficult to calculate because the colliding protons are not fundamental particles. Instead, protons are composed of quarks which carry fractional momentum of the total proton momentum. This fractional momentum is different depending of the particular circumstances, so physicist has created a tool that handles this difficulty, called the parton model.

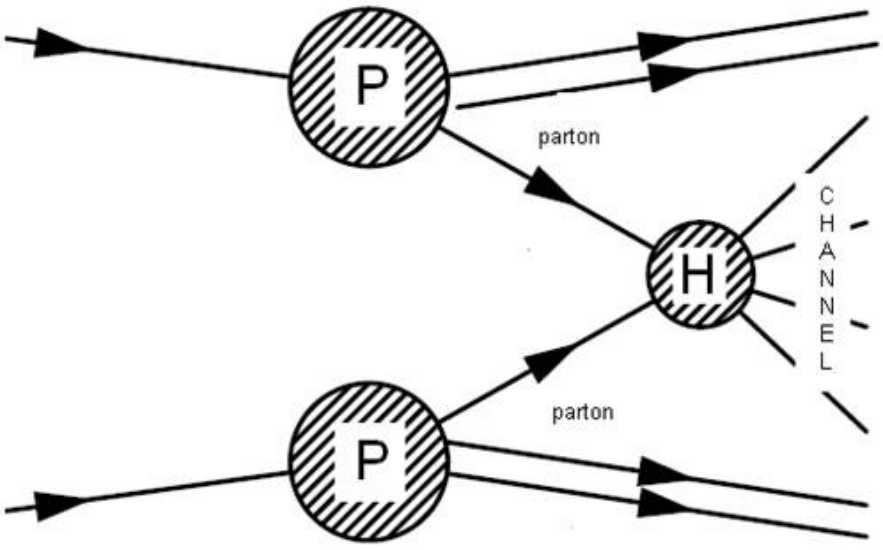

Figure 2.3 Parton-Parton interaction.

Higgs particles from P-P collisions will be created when two of the proton's quarks and gluons interact inelastically with the other proton's quarks and gluons. These kind of processes are better understood and described in terms of parton energy distributions where some fractional amount of energy will be carried by the proton constituents (partons). Figure 2.3 depicts this kind of process.

The calculation of a parton distribution function (PDF) is again non trivial, but it is very important if we want to calculate the cross section for important processes. Several physics groups work specifically on this kind of calculation. The cross section of parton-parton processes is given by equation 2.4 where "f_1" and "f_2" represent the PDF's, "Q" represents the momentum transferred and "x_1" ,"x_2" are the fraction momentum defined as: $x = \vec{p}_{parton} / \vec{P}_{hadron}$.

$$\sigma = \int f_1\left(x_1, Q^2\right) f_2\left(x_2 Q^2\right) \sigma_{parton}\left(x_1, x_2, Q\right) \tag{2.4}$$

The choice of which channels are the most useful for Higgs searches is given by the signal rates and the signal-to-background ratios in the various mass regions. Some of the most promising Higgs decay channels are:

- $H \to \gamma\gamma$
- $H \to b\bar{b}$
- $H \to ZZ \to 4\mathrm{l}$
- $H \to ZZ \to 2\mathrm{l}\, 2\nu$
- $H \to ZZ \to \mathrm{l}\, \nu 2\, jets$

Figure 2.4 shows the estimated discovery potential for various Higgs channels in the ATLAS detector for 100 GeV < $mass_{Higgs}$ < 1 TeV for an integrated luminosity of 100 fb-^{1}

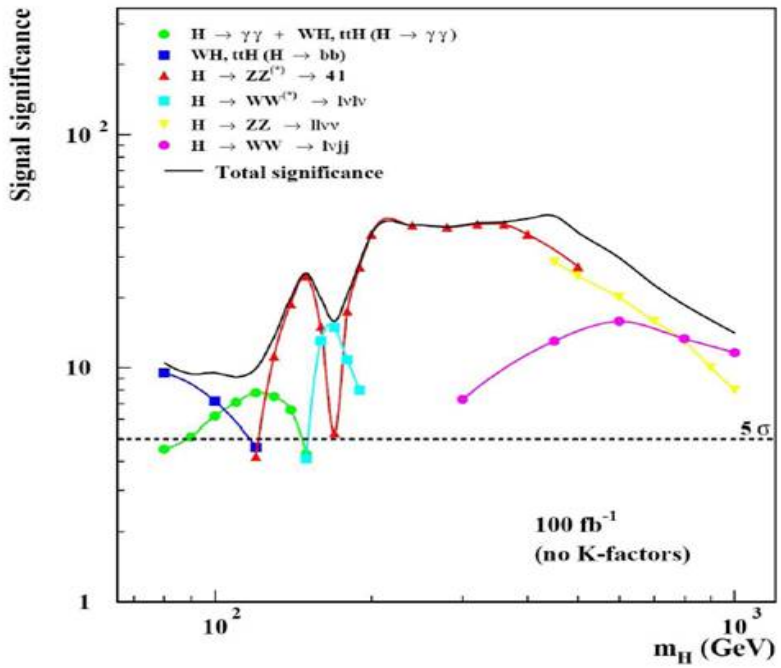

Figure 2.4 Sensitivity for the discovery of a Higgs boson.

2.3 Supersymmetry

The mass of the higgs boson, which is unspecified by the theory, is expected to be in the range 50 GeV<mH<1 TeV. Based on this argument, it is expected that experiments in the LCH confirm the existence of the higgs, but there is absolutely no guarantee that it will happen. Even if the higgs particle is found, it can be a non SM higgs particle. Instead it can be a particle that matches predictions from other theories. These theories have been developed in parallel with SM theories, and they are consistent with it. They are also waiting for confirmation once the LHC start providing experimental data. One of the most important of these alternative theories is known as

SUSY or supersymmetry. If SUSY exists at the weak scale, then supersymmetric particles will be discovered at the LHC. ATLAS can make measurements of SUSY masses and use them to infer properties of the underlying SUSY model.

SUSY predicts a partner particle for each of the particles in the SM. These particles, called "sparticles", should have exactly the same quantum numbers as their respective partners except for the spin and mass. SUSY's particles masses need to be much higher than the SM particles or otherwise we would have already found them in previous experiments. This explains why supersymmetry is called a broken theory.

There are certain rules for assigning to any particle the corresponding sparticle. For example, for each quark there should be a squark; for each lepton there should be a slepton; and similarly, the carrier particles should have their own SUSY partners, such as a gluino for each gluon, a neutralino for each neutrino, a photino as the partner of the photon, the W and Z particles have winos and zinos as partners respectively. Finally the higgs particle will have a higgsino. Figure 2.5 shows the correspondence between the two set of particles.

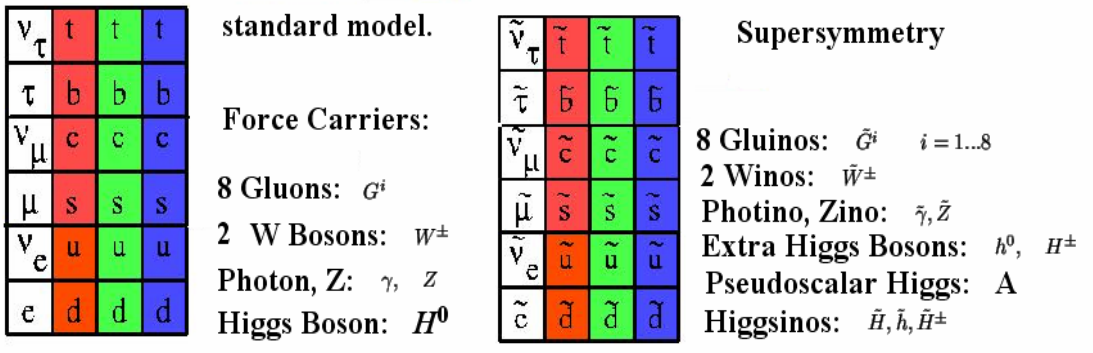

Figure 2.5 The standard model and SUSY particles.

Physicists are very interested in SUSY because it provides a particle candidate for dark matter. This particle is the LSSP, the lightest supersymmetric particle, and has no possible decays, and

therefore is stable. In addition to the previous discussion, supersymmetry also improves (compared to the SM) the search for GUT's (grand unification theories) and gauge couplings at the 10^15 GeV scale.

Supersymmetry offers the only presently known mechanism for incorporating gravity into the quantum theory of particle interactions. Some of the SUSY sub-theories such as SUGRA or super symmetric gravity and MSSM Minimal supersymetric SM, provide an elegant cancellation mechanism for the divergences affecting the higgs mass. This allows a unification of the three couplings of the gauge interactions at a high scale, but it does to a very highly cost of introducing many more parameters than the SM, at least 110 in the case of MSSM.

2.3.1 The MSSM

The Minimal Super Symmetric Model is referred as a minimal because it is the smallest extension of the SM that introduces supersymmetry, while being still consistent with the experimental data. The SSSM introduces the term "chiral" which correspond to any left and right hand spinors. In the MSSM each chiral fermion $F_{L,R}$ has a scalar Sfermion partner $\tilde{F}_{L,R}$ and each massless gauge boson A_μ with two helicity states ±1 has a massless spin-1/2 gaugino partner with helicity ±1/2. The complete list of all particles is shown in Table 2.2.

All the SM particles can be placed into MSSM multiplets. For example only the chiral and the gauge multiples are required to generate all fermions and boson plus the higgs particle. In addition the scalar partners are often given the labels "right and left". This is not related with the right or left handedness but rather with the fermion partner's helicity. Another feature of the MSSM theory is that it introduces five different physical higgs bosons: a charged pair of scalars higgs: $H^{\pm}$, a pair of neutral scalars higgs: H, h, and a neutral pseudo scalar: A. Their spin half

partners are the higgsinos. They can mix together with the binos and winos to create charginos $\tilde{\chi}^{\pm}_{1,2}$ or neutralinos $\tilde{\chi}^{0}_{1,2,3,4}$.

Table 2.2 MSSM list of particles.

Chiral supermultiplets in the MSSM			Vector supermultiplets		
Name	Spin 0	Spin 1/2	Name	Spin 1/2	Spin1
squarks, quarks	$\tilde{Q}=(\tilde{u}_L,\tilde{d}_L);\tilde{u}_R;\tilde{d}_R$	$Q=(u_L,d_L);u_R;d_R$	gluino, gluon	$\tilde{g}$	g
sleptons, leptons	$\tilde{L}=(\tilde{\nu},\tilde{e}_L);\tilde{e}_R$	$L=(\nu,e_L);\bar{e}_R$	winos, W's	$\tilde{W}^{\pm}$, $\tilde{W}^{0}$	$W^{\pm}$, W^{0}
higs, higsinos	$H_U=(H_u^{+},H_u^{0})$ $H_d=(H_d^{0},H_u^{-})$	$\tilde{H}_U=(\tilde{H}_u^{+},\tilde{H}_u^{0})$ $\tilde{H}_d=(\tilde{H}_d^{0},\tilde{H}_u^{-})$	bino, B	$\tilde{B}$	B

2.3.2 mSugra

Minimal supergravity is one of the most popular SUSY models. It assumes that that super symmetry breaking occurs through a gravitational coupling in its simplest form and only a limited number of parameters are required to give a reasonable approximation to others more extensive models. For example MSSM includes more than 110 free parameters, while Msugra has just four. They are shown in Table 2.3

Table 2.3 mSugra free parameters.

mSugra parameter	Description
m_0	Common Scalar mass
$m_{1/2}$	Common gaugino mass
A_0	Common trilinear Coupling
B_0	Common bilinear coupling

mSugra and the rest of Susy models including MSSM do not distinguish between quark lepton fields and higgs fields, so baryon lepton number violation are in principle not excluded. One way to fix this problem is the introduction of R parity conservation. RP is a discrete global multiplicative symmetry defined in equation 2.5.

$$R_P = (-1)^{3B+L+2S} \tag{2.5}$$

B is the baryon number, L is the leptonic number and S corresponds to the spin of the particle. In this way all SM have R parity RP=+1 and all supersymetric partners have RP=-1. In R parity conserving models all sparticles can only decay producing pairs where Rp is conserved with an odd number of sparticles. In this way the LSP is stable and becomes a strong candidate for explaining the invisible dark matter.

CHAPTER 3

COMMISIONNING AT THE TILE CALORIMETER

Before the ATLAS detector can be turn on, a long process of commissioning took place along, commissioning refers to the process of construction, testing and tune up of the detector. More than 1000 people among physicist and engineers work together in an international effort to set up the best conditions for the ATLAS detector within the right schedule. The next chapter will describe my personal contribution to the commissioning process during the 2006 and 2007 summers.

3.1 Component Description

3.1.1 The Low Voltage Power Supplies (LVPS)

LVPS are are among the most sensitive parts inside the Tile Calorimeter components that control the good performance of the system. As it was explained in a previous chapter all the electronics are contained into the removable super drawer at the external side of a module. Among all the electronic components we will find inside the drawer are the low voltage power supplies which control the phototubes. It is necessary to understand that the fingers are by themselves part of the modules, and they comprise all the electronics responsible to control their own module and no any other.

The Low Voltage Power Supplies or LVPS were built at CERN but before installation inside the ATLAS cavern the LVPS must be tested many times with a specialized hardware that simulates the actual situation of the LVPS at the detector. Once a LVPS is installed at it final position in the detector it is constantly monitored by the same kind of software we used for quality control, it can detect any wrong behavior and it can determine if is necessary to turn off the LVPS to avoid any further damage or if it just need a small correction of the internal components. Figure 3.1 shows a photograph of one of LVPS during the assembly process.

Figure 3.1 Low Voltage Power Supply (LVPS).

3.1.2 LVPS Bricks

There are 64 LVPS per partitioning (one LVPS per module) and four different partitions (LBA,LBC, EBA and EBC), makes a total of 256 LVPS in the detector, there are many more not installed but rather stored a the local CERN warehouse. Those LVPS are ready just in case we need to replace one of the installed LVPS. Every LVPS has eight different channels that control

different module subsystems. They are:+3.3V Digitizer (3Vdig), +5V Digitizer (5Vdig). +5V Mother Board (5VMB), -5V Mother Board (-5VMB), +15V Mother Board (15VMB), +5V High Voltage (5VHV), +15V High Voltage (15VHV) and -15V High Voltage(-15HV). The total number of bricks installed on the detector is 256 X 8= 2048 bricks that need to be constantly monitored.

Any of these channels is know as a brick and provides an specific Voltage to the corresponding subsystem, and it is expected that the voltage provided remains stable during most of the operational time. Small variations will occur depending on the subsystem behavior (if some devices turned on a small drop in Voltage during a short time can happen) nevertheless voltage variations can be critical and can cause a system failure in the worst case scenario. For example if the Voltage variation starts rising above a threshold voltage a security trigger system is activated and the brick is deactivated; this is what is known as a trip.

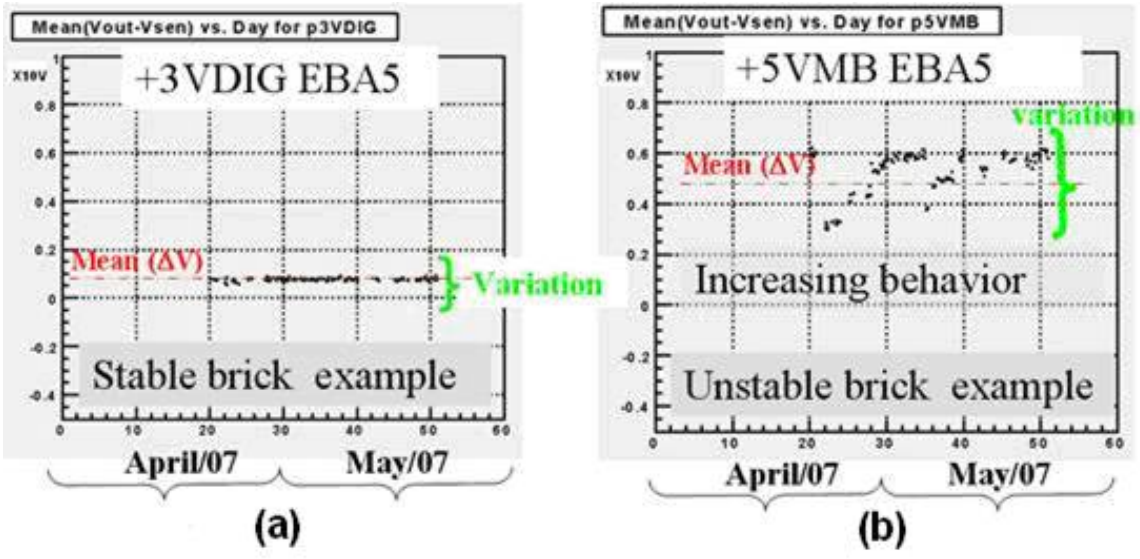

Figure 3.2 Two different bricks at EBA. (a) a stable brick (b) an unstable brick.

Figure 3.2 shows two different examples of “good” and “wrong’ behavior, the two examples correspond to the same LVPS located in the Module 5 EBA partition, in (a) the 3 Volts digitizer

voltage lies always close to its 3V nominal value with a voltage variation of less than ± 0.03V (less than 3%) so it is a stable brick, and this brick will need no further analysis if no trips are register for a long period of time. On the other hand Figure 3.2 (b) shows a 5V Mother Board brick with a large variation in Voltage. It goes from 3V to 6V (60%), so this is an unstable brick, and we need to be able to identify what is producing this kind of voltage variation in order to find future solutions. An unstable brick will have certain behavior or pattern that is important to recognize. It is not the same if a brick is unstable because of an internal electronic failure or because of is trying to respond to load changes from the circuit. For example in Figure 3.2 (b) between the days April 21st and May 10th the voltage starts growing from a nominal 3V (mean) to 6V, and because the Voltage was that high the brick tripped. It was reset again to it nominal voltage 3V. Unfortunately the same behavior happened later, and consequently more frequent trips were happening too. This was affecting the overall performance of that particular module, so identifying this kind of behavior becomes the most important part of this task.

This study does not involve the total amount of LVPS that the ATLAS detector because of several reasons: At the time of performing this analysis at CERN not all the LVPS were installed into their modules; Some of the already installed LVPS were turn off; Many others have already been removed because they reported bad behavior and they needed to be send back to repair. Finally we found no data in the following modules: LBC 14, LBC19, LBC 35-35 and LBC 39-60. In conclusion, a total of 25 modules out of 128 (EBA +LBC) have been studied, and particularly we present here, 5 bricks in full detail, they are: +3VDIG, +5VDIG, +5VMB, -5VMB and +15VMB.

3.2 The Online Status (TOS) and the Long Run Databases

The Online Status is the interactive version of the Data base which contains all the information about every module inside the Tile Calorimeter. It includes all the bricks from the LVPS for the

last two years, so we can always access this information and read any useful data about its current performance. The online status data base was created by our colleagues also working in commissioning. They have to monitor the modules after installation and during running, and any misbehavior should be written into the electronic log which is later updated and uploaded so it can be reviewed by the rest of the collaboration. Figure 3.3 shows an example of one of these internet table pages.

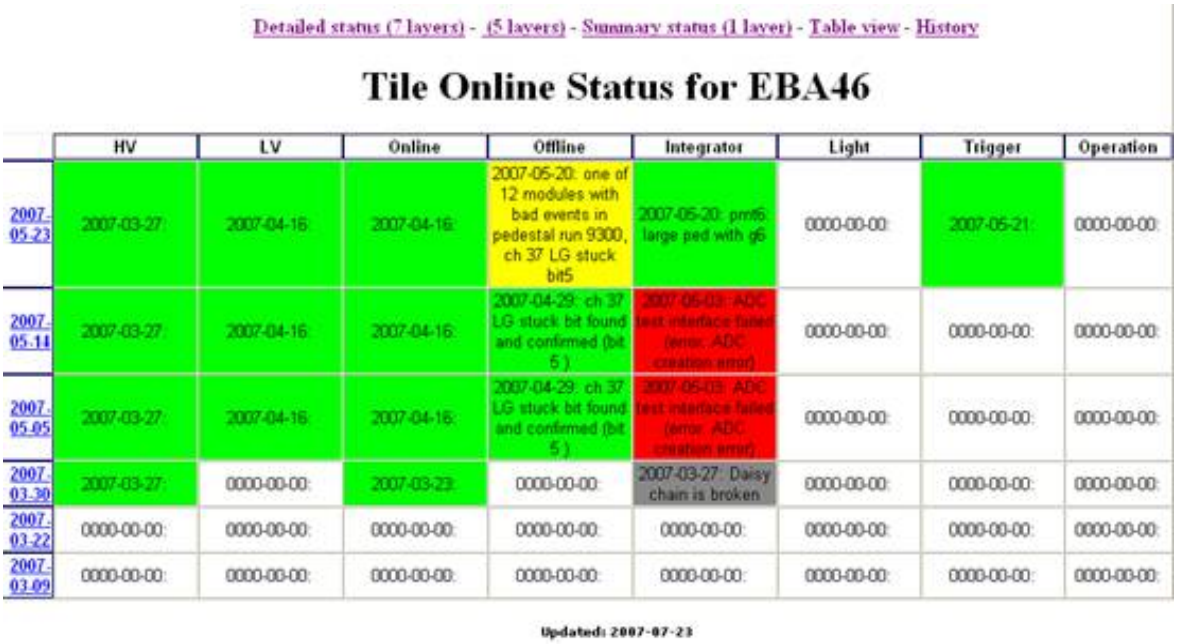

Detailed status (7 layers) - (5 layers) - Summary status (1 layer) - Table view - History

Tile Online Status for EBA46

	HV	LV	Online	Offline	Integrator	Light	Trigger	Operation
2007-05-23	2007-03-27:	2007-04-16:	2007-04-16:	2007-05-20: one of 12 modules with bad events in pedestal run 9300, ch 37 LG stuck bit5	2007-05-20: pmt6: large ped with g6	0000-00-00:	2007-05-21:	0000-00-00:
2007-05-14	2007-03-27:	2007-04-16:	2007-04-16:	2007-04-29: ch 37 LG stuck bit found and confirmed (bit 5.)	2007-05-03: ADC test interface failed (error: ADC creation error)	0000-00-00:	0000-00-00:	0000-00-00:
2007-05-05	2007-03-27:	2007-04-16:	2007-04-16:	2007-04-29: ch 37 LG stuck bit found and confirmed (bit 5.)	2007-05-03: ADC test interface failed (error: ADC creation error)	0000-00-00:	0000-00-00:	0000-00-00:
2007-03-30	2007-03-27:	0000-00-00:	2007-03-23:	0000-00-00:	2007-03-27: Daisy chain is broken	0000-00-00:	0000-00-00:	0000-00-00:
2007-03-22	0000-00-00:	0000-00-00:	0000-00-00:	0000-00-00:	0000-00-00:	0000-00-00:	0000-00-00:	0000-00-00:
2007-03-09	0000-00-00:	0000-00-00:	0000-00-00:	0000-00-00:	0000-00-00:	0000-00-00:	0000-00-00:	0000-00-00:

Updated: 2007-07-23

Figure 3.3 Example of a TOS webpage for April 2007 Module 46 EBA partition.

Based on this kind of information we collected the important data about the different LVPS in our own Excel spreadsheet. It is just a matter of collection and review one by one of all the TOS. There is also additional information from other parts that sometimes is useful and can be added to our own information, specially a data base called The Long Run. This database is a series of plots showing continuously the voltages of the bricks (Figure 3.3 is an example of one the plots from Long Run Database). Based on those plots we can identify the different behaviors in the voltages.

We found four different main behaviors and we can summarize them into categories. For all the LVPS we read the information from the Long Run data base and then tried to fit that information into one of the following categories:

Table 3.1 Different brick categories for the Long Run database.

Category	Behavior	Color
1	Big drops and unstable (DV>0.5V and variation>0.1V).	red
2	Normal drops and unstable (DV<0.5 and variation>0.1V)	yellow
3	Big drops and stable (DV>0.5V and variation<0.1V)	Orange
4	Normal drops and stable (DV<0.5 and variation<0.1)	Green

Category 1: A brick with very bad behavior, not only, it is not stable (does not remain at its main voltage) but it has big voltage drops or increments, which means that the actual voltage is way above or below (the average fluctuation) the nominal voltage and the variations are more than 0.5 around the nominal value. The color red is assigned to indicate that is something wrong and immediate attention should be provided.

Category 2: A brick which provides a main voltage value that is acceptable for us (within a range of 0.5V from the nominal voltage) but some times the variations are high enough to make it unstable. The main difference with category one is that category 2 will not create trips. A yellow color is assigned to this category to represent a brick that needs attention, but it is not potentially dangerous for the system.

Category 3: A brick which has few or no voltage variations but the main voltage provided is far away for the nominal voltage. An orange color is assigned because it will not jeopardize the

system, but the voltage should be fixed to the nominal voltage to assure good system performance.

Category 4: Represents those bricks with adequate behavior.

3.3 The Data collecting process

After the information was collected, we put it together in an Excel spread sheet. Figure 3.4 shows a small part of this kind of Excel sheet. In this case we only show one of the five bricks under study and only the first 15 modules from EBA. The table continues down with the rest of the modules (up to 64). After we complete them all, we start again but this time with 64 LBC modules. The table also continues to the right with the other 4 bricks. Additional tables are created for different dates, depending if the study is performed for just a week of run, a month, or more than one month.

date:	+3VDIG				
04/01-05/20	Vo-Vs	trend	Iout	trend	Integrator: large pedestal 5-23, offline: OK
EBA01	0.05	stable	4.2	unstable	Integrator: large pedestal
EBA02	0.08	stable	3.8	unstable	offline: low tails; Integrators: large pedestals
EBA03	0.18	stable	4.5	stable	no bad comments
EBA04	0.18	stable	4.8	stable	Offline: one bad channel; Integrator: Drawer ca
EBA05	0.05	stable	4.0	stable	Offline: several probles Noisy, correlated, Not a
EBA06	0.05	stable	4.5	stable	no bad comments
EBA07	0.1	unstable	4.5	unstable	Offline: Noisy and correlated
EBA08	0.1	stable	4.0	stable	no bad comments
EBA09	0.1	stable	3.8	stable	offline noisy,Integrator :long pedestal (only afte
EBA10	0.05	stable	4.0	stable	no bad comments
EBA11	0.1	stable	3.8	stable	several problems in both offline and integartor t
EBA12	0.1	stable	4.0	stable	offline: HG noisy , triple peak; Integrator: light l
EBA13	0.2	stable	4.0	unstable	comments says "everything screwed"
EBA14	0.1	stable	4.1	stable	no bad comments
EBA15	0.18	stable	4.0	stable	no bad comments

Figure 3.4 First 15 Modules of the +3VDigitizer brick from April to May (2007).

The first column in Figure 3.4 shows the name of the modules including the partition they belong to; also the color depends on the categories we explained before. The second column; “Vo-Vs” is the voltage difference between the current voltage of the brick and the standard voltage required (for example 3V for the +3VDIG brick); the next column “trend” will categorize the brick among one of the four categories we previously described in Table 3.1.

The “Iout” column represents the current provided by the brick and is only important if the brick is in the red category and is unstable. The last column is the comments found in the “TOS” web page. Their color category for this particular column is not decided by us but by the “TOS” responsible manager. The goal here is to see if there is any kind of relationship between the voltage difference, the trends or the comments found in the “TOS”. For example we can find that in a certain brick, the voltage difference (average) is correct but the delivered current is abnormal (there are also some design parameters which allow us to decide when a current has a non normal value). In this case we check the “TOS” comments and try to look for some explanation or correlation there, any clue that let us understand the cause of this behavior. Sometimes we find bad comments in “TOS” but nothing wrong with the other indicators, as the current, the voltage average, or the erratic trend. In these cases further analysis is required. If no relationship is found between voltage trend and the comments, the LVPS needs to be replaced or removed.

Table 3.2 EBA partition results for the summation of all bad categories.

	+3VDIG			+5VDIG			+5VMB			-5VMB		
LONGRUN	"TOS"	"TOS"	"TOS"	"TOS"	"TOS"	"TOS"	"TOS"	"TOS"	"TOS"	"TOS"	"TOS"	"TOS"
1	0	0	0	0	0	0	13	1	1	1	0	0
2	0	0	0	0	0	0	12	5	1	12	7	1
3	0	0	0	0	0	0	2	0	0	1	0	0
4	48	11	5	48	11	5	21	5	3	34	4	4
total	48	11	5	48	11	5	48	11	5	48	11	5
date:	+3VDIG			+5VDIG			+5VMB			-5VMB		

We collected all the information available, and then we were able to create tables as shown in Table 3.2, where we create a summary for four different bricks over the 64 different modules on EBA.

Table 3.2 shows the summation results over all the modules, and it summarizes the behavior of the bricks. The left column shows the categories from Table 3.1 according to the Long Run dataset. The second top row on the other hand shows the same kind of information but based on the “TOS” web pages categories given by our colleagues.

Finally, the idea is to cross check results from two different sources and try to identify any correlation; if that correction is found then we have detected the problem in the brick and we can process the next one. There are two ways that we selected modules for further analysis: either they are in the Category one, in Long Run or they are in red in “TOS” and not in Category 4 in Long Run at the same time.

The results for the digitizers are similar, no modules were found in category 1 in the Long Run database and all of the red in “TOS” belong to category one in Long Run, so no LVPS are wrong for this brick. A different story is happening with +5VMB where 15 LVPS are category 1 Long Run plus one more brick which is both; red in “TOS” and category 2 in Long Run Those 16 modules become part of the group that will undergo further investigation and they should be analyzed individually. Finally the -5VMb group contains only two problematic bricks, one red in category 1 Long Run and another one in category 2 Long Run plus red in “TOS”.

Table 3.3 LBC partition results for the summation of all bad categories.

	+3VDIG			+5VDIG			+5VMB				-5VMB	
LONGRUN	"TOS"	"TOS"	"TOS"	"TOS"	"TOS"	"TOS"	"TOS"	"TOS"	"TOS"	"TOS"	"TOS"	"TOS"
1	0	0	0	0	0	0	2	2	4	4	1	2
2	0	0	1	0	1	0	3	1	0	2	1	1
3	1	1	0	0	2	0	5	2	0	1	3	0
4	17	6	4	18	4	5	8	2	1	11	2	2
total	18	7	5	18	7	5	18	7	5	18	7	5
dates:	+3VDIG			+5VDIG			+5VMB				-5VMB	

Table 3.3 shows the same kind of analysis for the LBC partition. We can see that this time the numbers of modules active are less that 64, this is because LBC LVPS were still under installation. The results are less dramatic for LBC; basically there is one module requiring attention for +3Vdig and extra eight for +5VMB and 8 for -5VMB.

3.4 Results

Figure 3.5 shows one the results presented at a local CERN commissioning meeting where a detailed study was requested. The counting is a cross check between the Long Run database and the “TOS” tile on line status database and was performed on two specific bricks +5VMB and -5VMB because as shown previously these two bricks presented the worse behavior. The same categories we presented in Table 3.1 apply for the Long Run data, however because a more detailed study was necessary, we requested an updated “TOS” database with better description of the bricks status . One week later the “TOS” group presented the results, now four categories (one category extra) were introduced with very detailed information describing specific brick problems. The new “TOS” categories can not be associated with any color; they just give information about the specific technical behavior of the bricks. Figure 3.5 presents the previous results.

EBA + LBC Both 5VMB

	1	2	3	4
A	1	1	0	4
B	3	6	1	12
C	10	9	2	12
D	0	0	0	8

A: BCID errors for DMV

B: Group in 3's 6's 12's pedestals, noisy channels, high RMS

C: Groups in 3's 6's 12's CIS) AMP/Q, e/q, tails !=1

D:SB's -stuck bit

1.Big drops and unstable (ΔV>0.5V and variation>0.1V)

2.Normal drops and unstable (ΔV<0.5 and variation>0.1V)

3.Big drops and stable (ΔV>0.5V and variation<0.1V)

4.Normal drops an stable (ΔV<0.5 and variation<0.1)

Figure 3.5 Summary of "TOS" classification for Mother Boards.

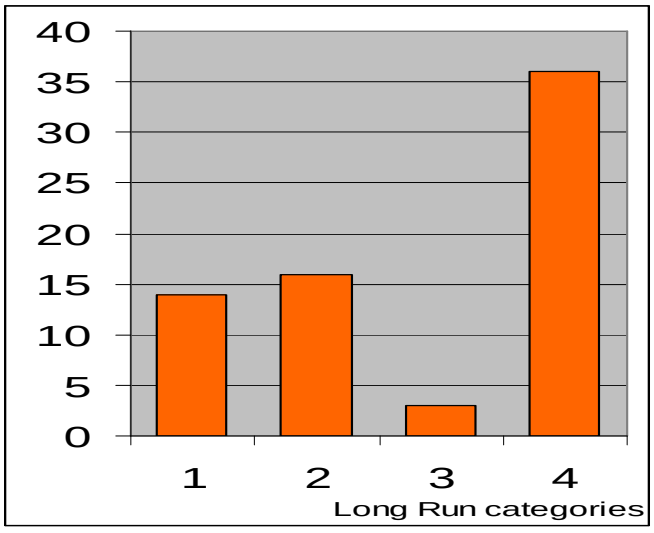

Figure 3.6 Total of 5VMB bricks of Long Run category.

Figure 3.6 summarizes the behavior of the both positive and negative 5VMB bricks. Information like this is also available for all the individual bricks for both databases and all four partitions. In

this specific example (one of the worst behavior cases) we see that the distribution of the bricks is having evenly divided behavior. These and many other plots are valuable results that have allowed us to understand how to identify and solve the LVPS problems that the commissioning process always will bring up.

CHAPTER 4

M5/M7 COSMIC STUDIES FOR THE ITC

Before collisions start taking place in the LHC ATLAS detector, different studies on the Intermediate Tile Calorimeter (ITC) cells are needed, and to achieve this, we can use the data collected during the Milestone cosmic rays Runs M5 and M7. During these runs, high energy muons went through the ATLAS detector and their path and energy deposition in the different cells of the Tile Calorimeter were recorded. The ITC cells are a subsystem of the ATLAS Tile Calorimeter as explained in chapter 2. They were developed and built at UTA; hence they are of special interest to our group.

4.1 The ITC Cells

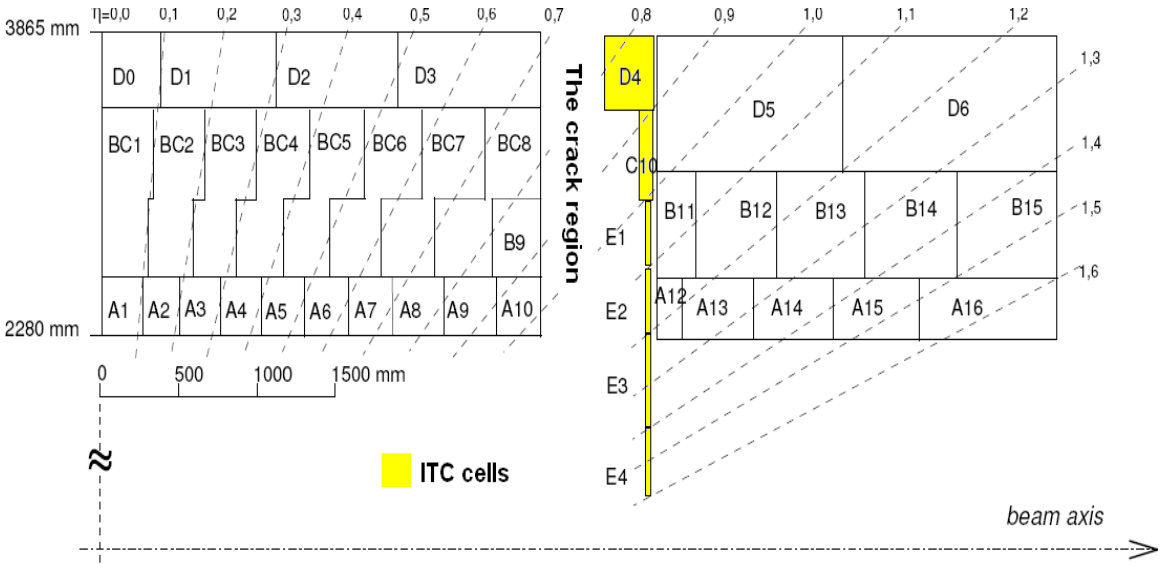

Figure 4.1 A quarter sector of Atlas Tile calorimeter.

The Intermediate Tile Calorimeter (ITC) cells are an addition to the long extended barrels, LBC and LBA cells systems, with the goal of maximizing the instrumentation of the detector in the service region (crack region). They are found within the range $0.8<|\eta|<1.6$. This position corresponds to the gap between the long barrel and the extended barrels ($z\approx3.5$m). Figure 4.1 shows a side view of all ITC cells in a single module for a long barrel and its extended barrel. Because of the azimuthal symmetry of the atlas detector, all of ITC cells will look the same in any particular module. ITC cells are painted in yellow, and every module contains six different ITC cells, whose names are: D4, C10, E1, E2, E3 and E4. As explained in chapter one, cells D4 and C10 use steel plus scintillating tiles while all E cells only contain scintillating material.

4.2 The M5/M7 datasets

The data sets belong to the cosmic runs M5 and M7. These are a long list of files created with information from the ATLAS cosmic runs taken in late 2007 and early 2008, during the Milestone week (M5 and M7). The data files contain information for most of the detector systems, including the muon system, the inner detector, the calorimeters and the ITC cells. The number of runs for M5 is about 100 and more than 1300 for M7. All runs are normally taken on different days and for different periods of time. We have selected two different runs; one for M5 and one for M7, each of them have more than 10000 events to assure a large amount of statistics.

The M5 dataset belongs to run 28940, which is located at “DISK TRIUMP” in Canada. It has also been locally saved to one of the UTA’s hard drives for easier access. The size of the data set is about 1000 Gb (1 Tb) and is arranged in a little more than 5000 partitions. Each of these partitions is 186 Mb with exactly 213 events per file. In total we have more than one million events. On the other hand, the M7 dataset belongs to run 69069. It has less files that M5, with

only 409 partitions, each with 280 events and 127 Mb, for a total of 51 Gb of total data. The M7 dataset is also located at UTA's local machine. The format used for both datasets is flat Ntuples which allows us direct analysis in ROOT without the need of further reconstruction as in the case of the raw data or AOD's.

The M5 file data set includes different triggers, one of which is the L1Calo trigger which is explained in [19]. This trigger allows the M5 recording system to save only cosmic muon events that passed across the detector. This fact ensures that the events we are reading have some similarity to those that would be created in the case of normal running conditions during PP collisions. The Tilecal coincidence boards are another trigger provided by the University of Chicago. This trigger connects 12 modules per partition on the region $\Phi>0$ (top region of the detector) and $\Phi<0$ (bottom region of the detector). When a certain number of cells, or clusters, detect activity at the same time in both sides (back to back) of the detector, information, like energy deposition, cell's location angles and transverse momentum, are recorded into the Ntuples.

M7 has the L1CaloTrigger plus the TileMuonFitter or TMF algorithm. This latter triggers works in the following way: for each event, a straight line is fit to the center of the cells that detected the energy deposition. The track positions are minimized using a function of the squares of the orthogonal distances of each cell to the track; this distance is weighted with the energy of each respective cell. A more detailed description of the TMF can be found in [20].

The Ntuples in ROOT are seen as TTrees which contain branches with several variables. These variables have information on different parts of the detectors, so not all are of our particular interest. In fact most of the information in the Ntuples needs to be ignored for our ITC cosmic

studies. Table 4.1 describes all the variables that we need to read from the M5/M7 datasets. Variables shaded in gray are called “Cell Container”.

Table 4.1 Important M7/M5 variables inside the Ntuples.

Name	Type	Description	Dataset
ECellTile	vector<float>	cell energy in MeV for each event	M5/M7
DetCellTile	vector<float>	Binary code, Identify sampling (A,BC,D)	M5/M7
EtaCellTile	vector<float>	Pseudorapidity position of the cell	M5/M7
PhiCellTile	vector<float>	phi position of the cell	M5/M7
NCellsTile	Int_t	Number of active cells in the event	M5/M7
TileCosmicsMT_phi	Double_t	Track phi position	M7
TileCosmicsMT_theta	Double_t	Track theta position	M7
TileCosmicsMT_x	Double_t	Coordinate of the y=0 plane crossing	M7
TileCosmicsMT_z	Double_t	Coordinate of the y=0 plane crossing	M7
TileCosmicsMT_cellSample	Int_t	0=A sampling, 1=BC sampling, 2=D sampling	M7
TileCosmicsMT_cellE	Double_t	Same as ECellTile, only for cell in TMF	M7
TileCosmicsMT_trackNcells	Double_t	Number of cells within a radius “d” of the track *	M7
TileCosmicsMT_fitQuality	Double_t	0= event fails cut, 1= event passes cut	M7
TileCosmicsMT_fitNcells	Int_t	Number of cells passing cuts	M7
TileCosmicsMT_energy	Double_t	Energy sum of cells in a radius “d” of the track*	M7
TileCosmicsMT_energyTop	vector<double>	Top modules energy sum in each sampling	M7
TileCosmicsMT_energyBottom	vector<double>	Bottom modules energy sum in each sampling	M7

M7 dataset contains, in addition to the Cell container variables, information on the muon reconstruction algorithm called “TileCosmicsMT”. These variables describe the path, energy

* For LBA,LBC; Asampling: d=300mm, BC sampling: d=375mm, D sampling: d=860 mm. For EBA and EBC; A sampling d=750mm, BC sampling: d=750mm and D sampling: d=1700mm.

deposition and cell information of the muon event. The “TileCosmics MT” variables are reconstructed directly from the “Cell Container” information according to the Muon Track algorithm, developed by Jose Maneira, and described in detailed in [20].

All of the previous variables are not difficult to handle except for DetCellTile. This variable contains information that needs to be translated first, since it is encoded into a 20 bit digital number, where every set of bits correspond to a particular part of the detector. In order to have a clear understanding, a decoding table is necessary before continuing with any other analysis.

Table 4.2 DetCellTile 20 bit binary code for cells in TileCal.

Decimal number	Cells Name	20 bit Binary Number Code					
65	Barrel Presampler	00	00	000	0000	00011	0101
81	LAr Front	00	00	000	0000	00101	0001
97	LAr Middle	00	00	000	0000	00110	0001
113	LAr Back	00	00	000	0000	00111	0001
65544	Tile Barrel A	00	01	000	0000	00000	1000
73736	Tile Barrel BC	00	01	001	0000	00000	1000
81928	Tile Barrel D	00	01	010	0000	00000	1000
131080	Ext Barrel A	00	10	000	0000	00000	1000
139272	Ext Barrel B	00	10	001	0000	00000	1000
147464	Ext Barrel D	00	10	010	0000	00000	1000
270344	TileGap C	01	00	001	0000	00000	1000
278536	TileGap D	01	00	010	0000	00000	1000
811016	TileGap E	11	00	011	0000	00000	1000
		Gap/Gap scintillator	LB/EB	Sample	FCAL/ HEC	EM’s bits	Calo bits
		TILE CAL					

The decoding was performed running a C++ algorithm that reads the DetCellTile information from the Ntuples and, at the same time, we extract from the “CellContainer” the EtaCellTile and the PhiCellTile position and then we write it into a text file. In the next step, we can easily match the code information with the position, based on the detector geometry and the ATLAS blueprint. Table 4.2 shows the code information for different calorimeter cells.

The first four bits that belong to the “Calobits” column, on the right, tells us which calorimeter the cell belongs to:

- 1st bit: Liquid argon electromagnetic calorimeter (EM).
- 2nd bit: Liquid argon hadronic end cap (HEC).
- 3rd bit: Liquid argon forward calorimeter (FCal).
- 4th bit: Tile calorimeter (TileCal)

The following 5 bits present information from cells in the electromagnetic calorimeter (EM):

- 1st and 2nd bits: sampling (00 for presampler, 01, 10, and 11, for each consecutive layer).
- 2nd bit: barrel.
- 4th bit: inner endcap.
- 5th bit: outer endcap.

The next four 4 bits provide information about the cells that belong to the hadronic end cap (HEC) and the forward calorimeter (FCal):

- 1st and 2nd bits: HEC sampling (00, 01 in the first wheel and 10, 11 second wheel).
- 2nd and 4th bits: FCal modules (00 for the EM; 01,10 and 11 for the 3 sampling hadronic)

Finally the last 7 bits correspond to these cells in the Tile Calorimeter:

- 1st, 2nd and 3rd bits: sampling (000 is A sample; 001 is BC sample; 010 is D sample; 011 is E sample; 100 is X sample).
- 4th bits: long barrel (LBA or LBC)
- 5th bit: extended barrel (EBA or EBC)
- 6th bit: gap iron (C4 and B10 ITC cells)
- 7th bit: gap scintillator (E1, E2 E3 and E4 ITC cells)

Before we continue it is very useful to present a very simple calculation (may be oversimplified) on the energy deposition by comics muons on the Tile calorimeter. The purpose here is just to have an estimate on this value in order to understand the units (which are not provided) that the M5/M7 Ntuples have for energy, and be able to read this information correctly. We have assumed a muon travelling in a direction such that it crosses the cells diagonally from corner to corner (maximum distance) and deposits 2 MeV per cm in the scintillator material and 1.45 MeV per cm while travelling through the iron, we also know that the iron/scintillator rate in the cells is 4.67. The values of deposition are taken from [3]. Table 4.3 shows the calculations.

Table 4.3 Energy deposition for different cells.

Cell Name	D4	D5	C10
Length (mm)	300	1250	100
Height (mm)	440	580	450
Width (mm)	200	200	150
Total distance $\sqrt{L^2+H^2+W^2}$	59.885	152.47	48.476
Dist. in scintillator @ 2MeV/cm	10.032	26.892	8.5496
Dist. in iron @ 1.45MeV/cm	46.853	125.58	39.927
Total Depot. energy (MeV)	88.002	235.88	74.993

4.3 Cosmic Analysis with M5 Dataset

The following section describes results where only the M5 data set was used. M7 data was not used at this time because it was not available until late 2008. We perform the analysis mainly looking at the energy deposition in ITC cells and comparing it with the energy deposition in other cells from the Tile calorimeter.

4.3.1 Position and Energy

Figure 4.2 shows a 2D energy histogram of Modules vs. Towers. We can see from the distribution of pseudorapidity that only one of the extended barrels is present (EBC).

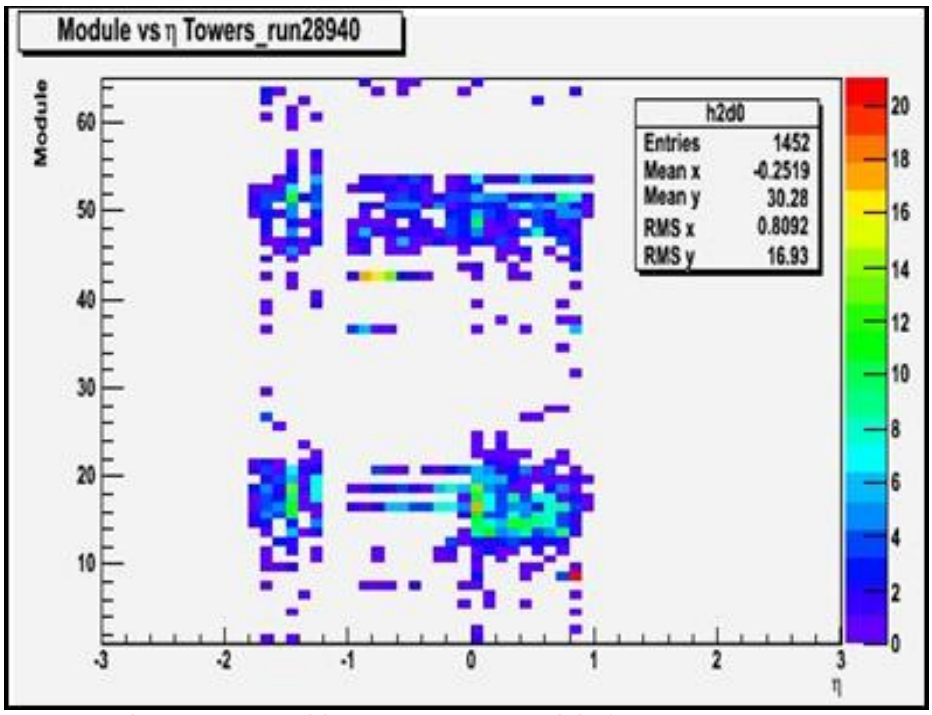

Figure 4.2 A 2D histogram eta vs module for energy towers.

The extended barrel, LBA, contains no data because at the time of the run, the commissioning process was still ongoing on the A side of the detector, turning off the LBA barrel. For the studies

of the ITC, only C side (negative pseudorapidity) can be taken into account. In addition we can see the presence of the Chicago coincidence board trigger, making the top and bottom regions, specifically from module 10 to 24 and 42 to 54, more populated (see Figure 4.2). The gap region is clearly present at a position $-1.1<\eta<-1$ where we also found the D4 ITC cell.

Figure 4.2 also shows that the η information is not compatible with the blue prints in Figure 4.1. For example, we expect the Long Barrel to be in the region $\eta<-0.8$ but the actual value is $\eta<-1.2$. The difference is at least a 0.3 shift in eta. This difference is because during the M5 run the nominal position in LBC was moved 1.5 meters outwards. Table 4.4 reflects this situation.

Table 4.4 Eta values on some cells.

Cell (C side)	D4	D5	C10	B11	E1	A12	E2
Nominal eta value	-0.8	0.9	0.9	1.1	1.1	1.2	1.2
Actual eta value	-1.1	-1.2	-1.2	-13	-13	-14	-14

4.3.2 Detecting cosmic events in ITC cells

The number of cells under study can be easily calculated; there are 6 ITC cells per Module and 64 Modules per partition in the C side of the ATLAS detector. We also include studies of 3 non ITC cells, D5, B11 and A12. So we have, in total, 576 ITC cells under investigation. The most important cells are those that meet trigger conditions, so that we can concentrate on modules 10 to 22 and 42 to 54, Top and Bottom of the detector respectively. However, the plots that we will present will include the total amount of data available, including those cells with poor statistics unless otherwise stated.

Adding cells which do not belong to ITC will help us to compare some of the behaviors between neighboring cells and will make the study more complete. We have included adjacent cells from the extended barrel (EB) so every ITC cell will have a counterpart in the EB. By doing so, we will be associating cell pairs like in Figure 4.3. Notice that because only 3 cells in EBC are immediately next to ITC cells, E3 and E4 will have no counterpart and D5 will be associated both with D4 and C10.

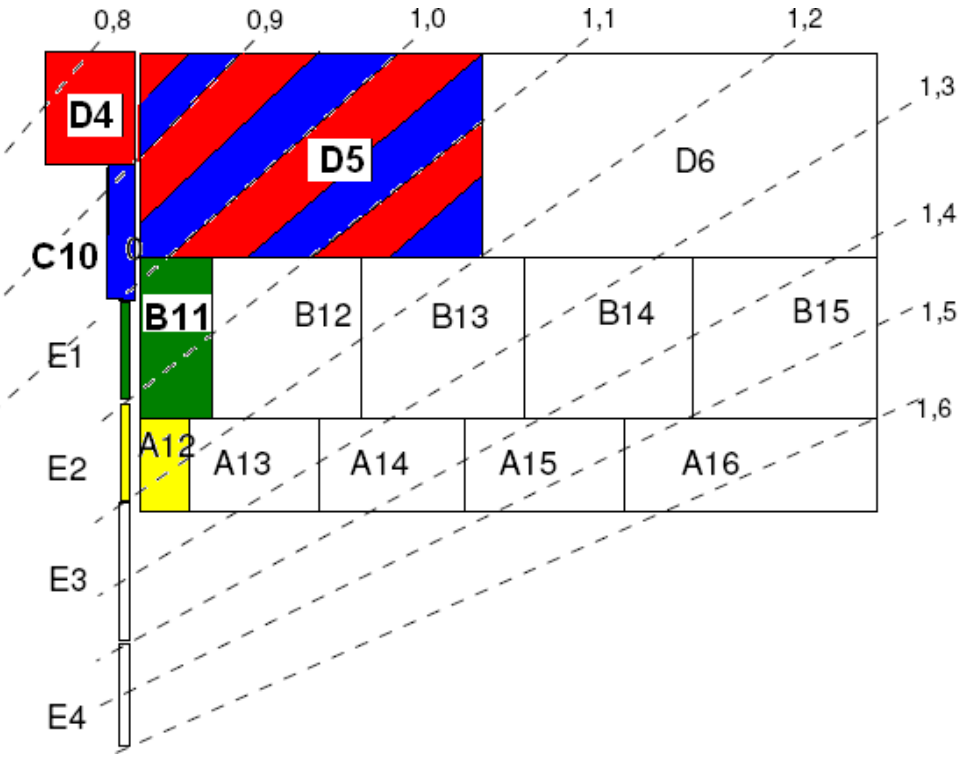

Figure 4.3 Associated Cells are shown with the same color.

We need to calculate the average energy deposition in the ITC cells produced by the cosmic rays crossing the detector. We also need the previous information for all the cells adjacent to the ITC cells in the EBC partition. This average needs to be calculated for every individual cell, so, in total we have 448 averages organized on a 64 by 7 matrix (modules x cells). The average calculation excludes all events with energies close to zero. A 200 MeV cut in energy is made, and the

selection of this cut is based on the noise level of the cells, which depends on the amount of active material that is present. It is also necessary to calculate the combined average energy deposition in the cell pairs (D4 +D5 for example), which give us another 64 by 8 matrix. The reason to include these combined pairs of cells is so that we can select simultaneous events in both cells, and we can isolate true events from fake events created by noise. Notice that, there are only 4 pairs of cells but 8 different pairs of energy averages. This is because the energy cut is applied on the first cell of the pair, so for example the pair “D4+D5” will be different than the “D5+D4” cell pair.

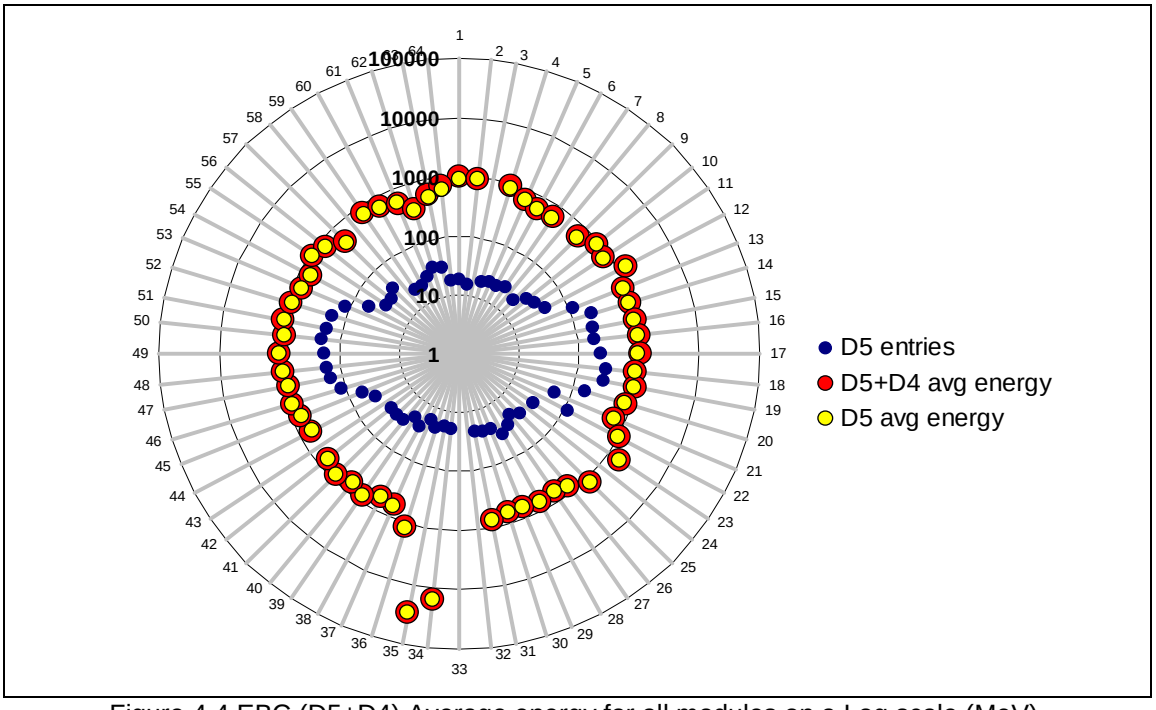

Figure 4.4 EBC (D5+D4) Average energy for all modules on a Log scale (MeV).

Figure 4.4 shows, in red, the cell pair (D5+D4) average energies for all modules in EBC. In this case, D5 is the selection for the energy cut. We also show in blue the number of entries. We can see clearly how the top and bottom cells (10 to 22 and 24 to 54) present more entries than the others modules. It is also clear that the average is similar for most of the modules with values that

are around 1000 MeV. There are some cells that have extremely high average energy (modules 34 and 35); we believe this behavior is introduced by some noisy channels. Finally, in yellow, averages for an individual cell (D5) overlap most of the time with cell pair (D5+D4). This fact indicates that D5 contains most of the energy entries (which is expected due to the bigger size of D5 cell). Figure 4.5 shows an energy cell plot for the case when we apply the energy cut on D4.

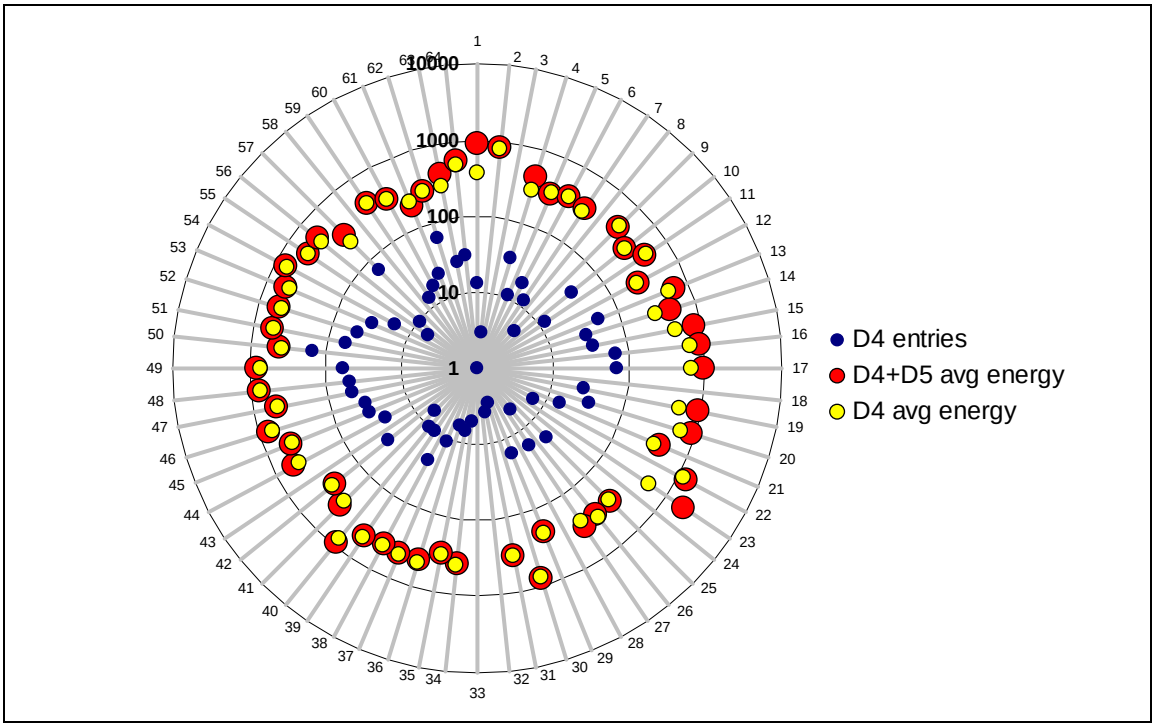

Figure 4.5 EBC (D4+D5) Average energy for all modules on a Log scale (MeV).

This time the plot shows different features. For example, there is more than one D4 cell with no entries, but this feature can be explained if there are cells that are turned off during the run. The distribution of the entries is not as clear as it was in Figure 4.4 where the top and bottom cells had the most number of entries. Finally, the cell pair average energies are, in most of the cases, greater than the individual cell energy. This means that the D5 energies are significantly larger than those in D4 in the same event. This can be explained if we recall that the sizes of the cells are directly related with the deposition of energy from the particles. Once the averages are ready,

we can introduce a variable called “signal”. This variable will be different for every individual cell and for every cell pair. We will calculate 64 x 7 individual signals and 64 x 8 pair signals. Below we show Equation 4.1 used for the case of cell pair D4+D5, and other cell calculations are similar.

$$signal(D4+D5) = \frac{D4energy + D5energy}{average(D4energy + D5energy)} \tag{4.1}$$

Equation 4.1 also uses an energy cut of 200 MeV on D4. This means that if on a particular event the energy on D4 is larger than the cut, then we proceed to calculate the “signal” value with the energy in D4 plus whatever energy is in D5, whether D5 energy is more than 200Mev or not. On the other hand, for the case of “signal (D5+D4)”, the 200 MeV energy cut will only apply to D5.

In summary we have created 8 plots:

Table 4.5 Plot description.

	Y axis	X axis	200MV cut by		Y axis	X axis	200MV cut by
1	Signal(D4+D5)	D4/avg(D4)	D4	5	Signal(D4+D5)	D5/avg(D5)	D5
2	Signal(C10+D5)	C10/avg(C10)	C10	6	Signal(C10+D5)	D5/avg(D5)	D5
3	Signal(E1+B11)	E1/avd(E1)	E1	7	Signal(E1+B11)	B11/avd(B11)	B11
4	Signal(E2+A12)	E2/avg(E2)	E2	8	Signal(E2+A12)	A12/avg(A12)	A12

4.3.3 M5 Results

Figure 4.6 shows two of the 8 plots described above (plot 1 and 5). We have circled in red some of the events that have outstanding values of the signal variable in (4.1) and represent energy deposition for the cell D4 and D5 respectively. Figure 4.6 (a), D4D5 pair cell, is mostly distributed on a thick straight line, whose values remain in the energy averages calculated previously. Also,

a large concentration of points is expected around the position (1, 1). However, a few of the points lay above the main line representing both high energies in D4 and D5. This is a sign that a high energy particle, mostly muons, traveled through both cells. When we make the same plot for the D5D4 cell pair (b), with a 200 MeV energy cut onD5, the results are slightly different. Figure 4.6 (b) reveals the same linear behavior but with less candidates over the line for cosmic events. We were expecting this kind of result because, as already explained, D5 will detect particles more often than D4.

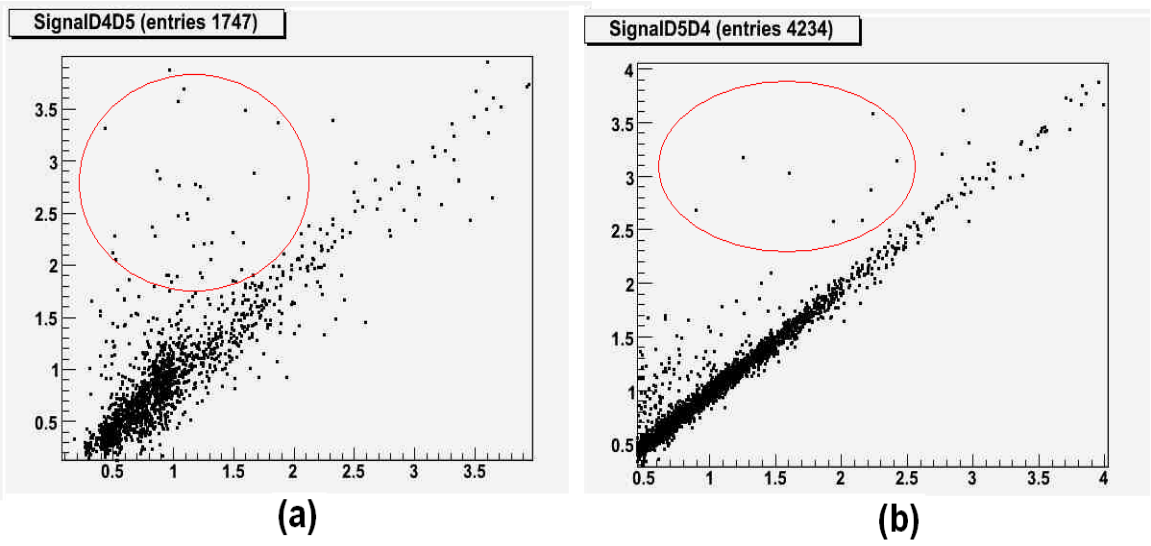

Figure 4.6 Cosmic ray detection by the D4D5 (a) and the D5D4 (b) pair cells.

We also have created plots where the “signal” value is plotted vs the module number for those cell pairs. By doing this we can determine the dominant path direction on muons path. Once again 8 plots were created in the same order as presented in Table 4.5. Figure 4.7 shows an example of these kinds of plots for the D4D5 cell pair in (a), and the D5D4 cell pair in (b). Once again we see a major distribution of the top and bottom modules (modules 10 to 20 and 45 to 55) so we can argue that most of the times the muons travel close to a vertical line through the detector (cells under study).

The values enclosed by the red circles are those where the signal values were relatively higher than the average energies, representing a detected cosmic event. The other six plots show similar behavior to the ones previously shown. They differ only in the number of statistics since different ITC cells have different sizes and the numbers of muons crossing them varies.

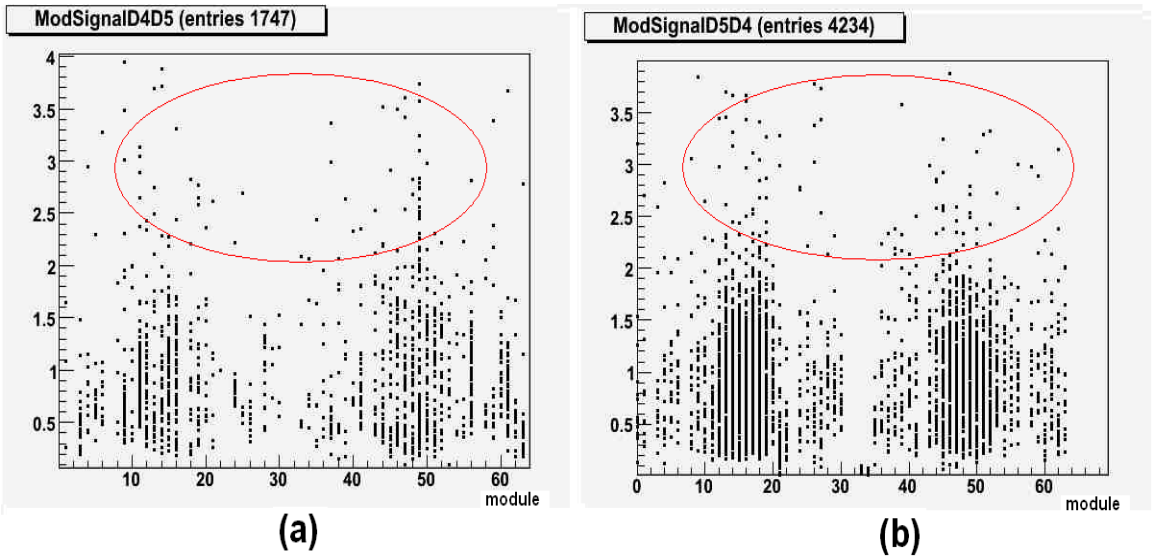

Figure 4.7 Energy signal vs. module for D4D5 (a), and D5D4 (b) cell pairs.

4.4 Cosmic Analysis with M7 Dataset

4.4.1 First Muon Tracks

In this part of the analysis we are working exclusively with the “TMF” variables. We have made two selections. We required the variable “fitNcells” has a value no less than six; this means at least 6 hits in different Tile calorimeter cells. The other selection is at least one hit on each of the three different samplings (variable”CellSample”). We show in Figure 4.8 a basic representation of

some of the muons passing across the tile calorimeter with their respective positions in theta and phi. In order to completely describe a muon track for different variables are required. In addition to the angles theta and phi, we also have the x,z positions that determine the intersection with the y=0 plane. This plane is the one that cuts in two half part the tile calorimeter (a cut from module 1 to module 32 in Figure 4.8). The plot shows a lateral view of the Tile Calorimeter so only information about theta can be seen explicitly.

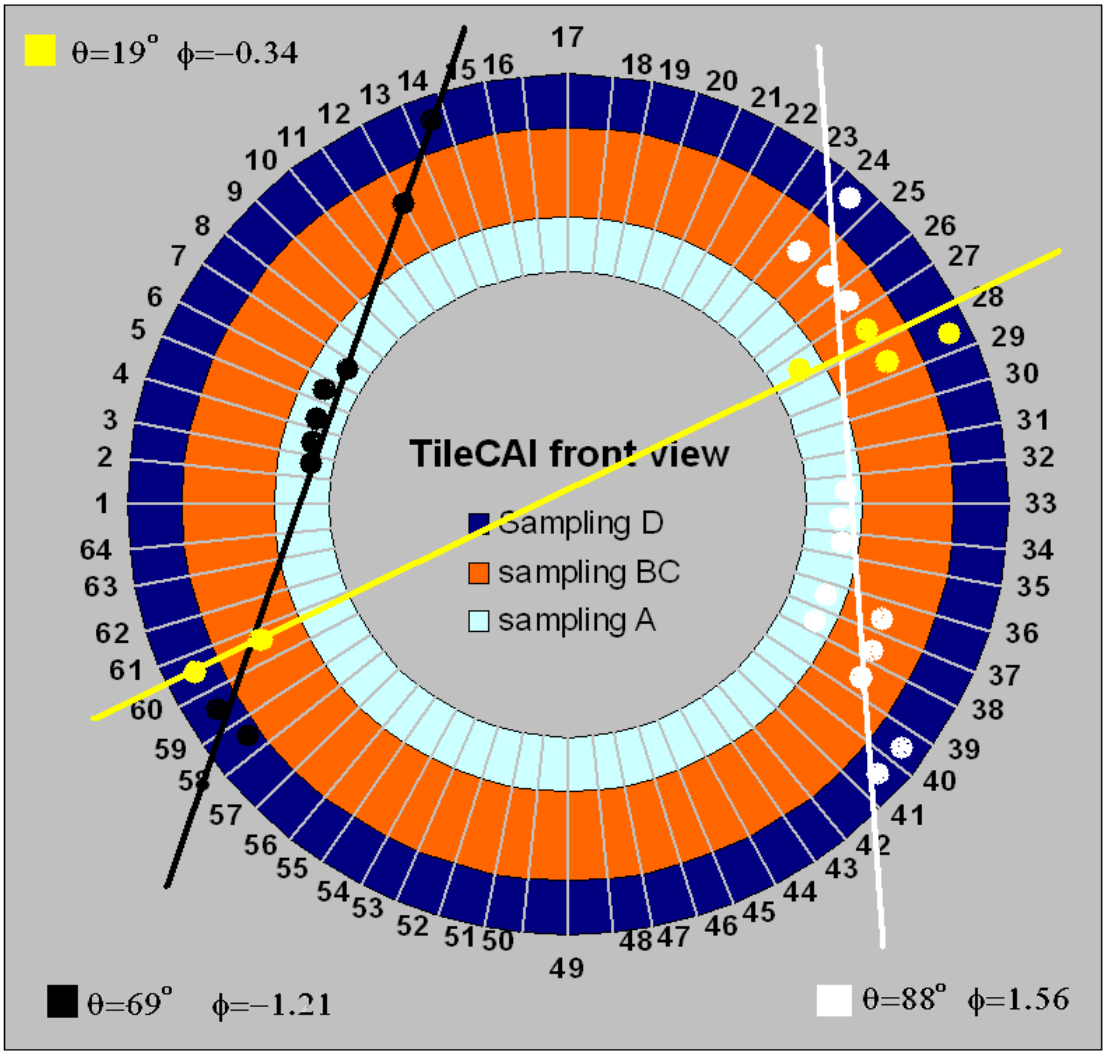

Figure 4.8 Some muon tracks in the tile calorimeter.

The most important feature that can be observed from Figure 4.8 is that the muon tracks, most of the time, will not cross the center of the detector (non projective tracks). If we want to study ITC cells then we have to be careful with non projective tracks because the information of pseudorapidity or eta in each cell from the same track will probably be different. That is the main reason that we need to use the “theta” position for muons track direction, instead of the most commonly used “eta”. Figure 4.9(a) shows the muon tracks distribution in the y=0 plane. As we can see most of the events are located in the hadron calorimeter and in the cylindrical cavity inside it. Some of the events will cut the plane beyond the TileCal dimensions, this shows once again that many of the track are non-projective, interacting with only a few external cells and then leaving the calorimeter. Figure 4.9(b) shows a phi vs theta plot. Here we can see the angle distribution of the tracks. Most of them are located in Φ=±1.6 or Φ=±90°, which are muons travelling completely vertical to the detector.

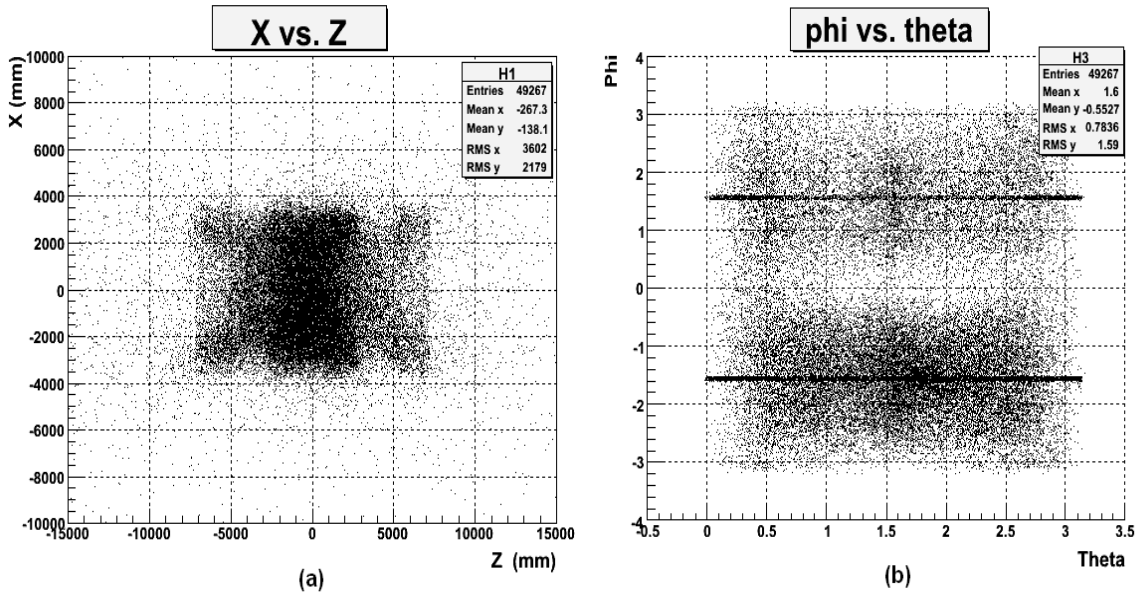

Figure 4.9 Muon track distributions. (a) x vs. z crossing points. (b) phi vs. theta tracks.

One more important aspect is that the “TMF” algorithm does not take into account information from the ITC cells for the muon track reconstruction. In spite of these difficulties we are still able to analyze the ITC cells’ response to the cosmic muons. The technique used, is very similar to the one described for M5 data. We use a pair of cells in the same module D4/D5, C10/D5, E1B11 and E2/A12 as we did before. Then we look for events passing through the non-ITC cells. Finally, we check the energy deposition in the corresponding ITC cell partner. In the next section we will show many of the results we can get using this technique.

4.4.2 M7 Results

Figure 4.10 shows the response to cosmic rays of one single D5 cell, in this case from module 17. We can observe that the histogram has a peak at about 1Gev due to the energy deposition of muons in the cell. We also applied an energy cut of 200 MeV to remove a large peak at 0 point energy generated by background noise.

The plot has been fitted with an exponential plus a Landau function, where p0 and p1 are the two parameters for the exponential function and p2 to p4 are the parameters of the Landau function. We have made plots as in Figure 4.10 for all D5 cells in all modules. Most of the module cells present a very similar behavior except for module 33, which presents no entries. We suppose this particular module was turn off at the time of M7 runs. It is interesting that if we try to reproduce the same kind of plot for cells D4 we do not get a similar result; instead, we get an exponential behavior with a long tail, where we believe, lies the information of the muon energy deposition, and we will try to prove it using the following arguments.

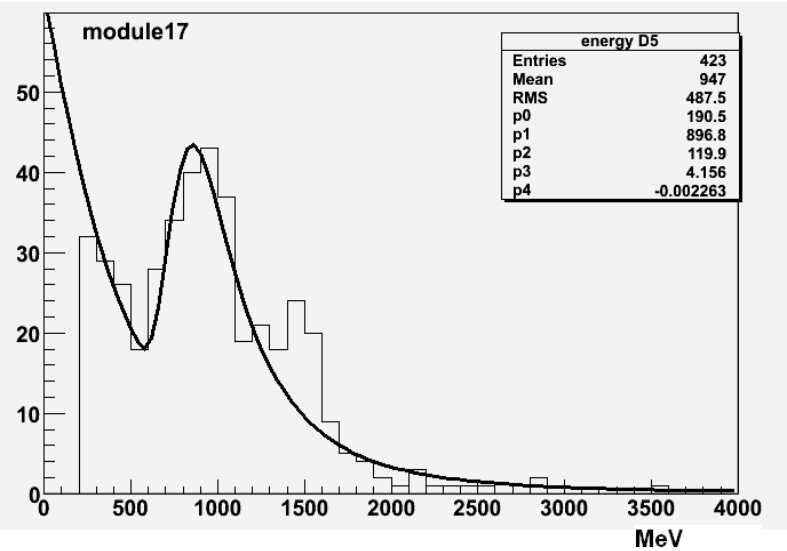

Figure 4.10 Response to cosmic ray, exponential + Landau fit.

Figure 4.11 shows four different examples of energy deposition in cells D5, D4 and C10 where the histograms have been superimposed on the same canvas. We are showing top modules, where the cosmic activity increases but the behavior is similar (with less statistics) for other modules. The information plotted is all from the “cell container” variables but the selections are made from the “MTF” variables in the following way: if there is a “MFT” track passing through any D5 cell, then we read in the same Ntuple event, and the energy information located in the “cell container” variable for D5 is plotted. Then we read D4 and C10 energies corresponding to the same module. We should remember that the ITC cells are not present in the “MFT” variables so the cell pair technique has to be used.

Figure 4.11 shows four examples of different modules in the C side of the detector, where the ITC energy deposition were plotted in the same histogram than the D5 energy entries that were selected by the muon fitter track algorithm

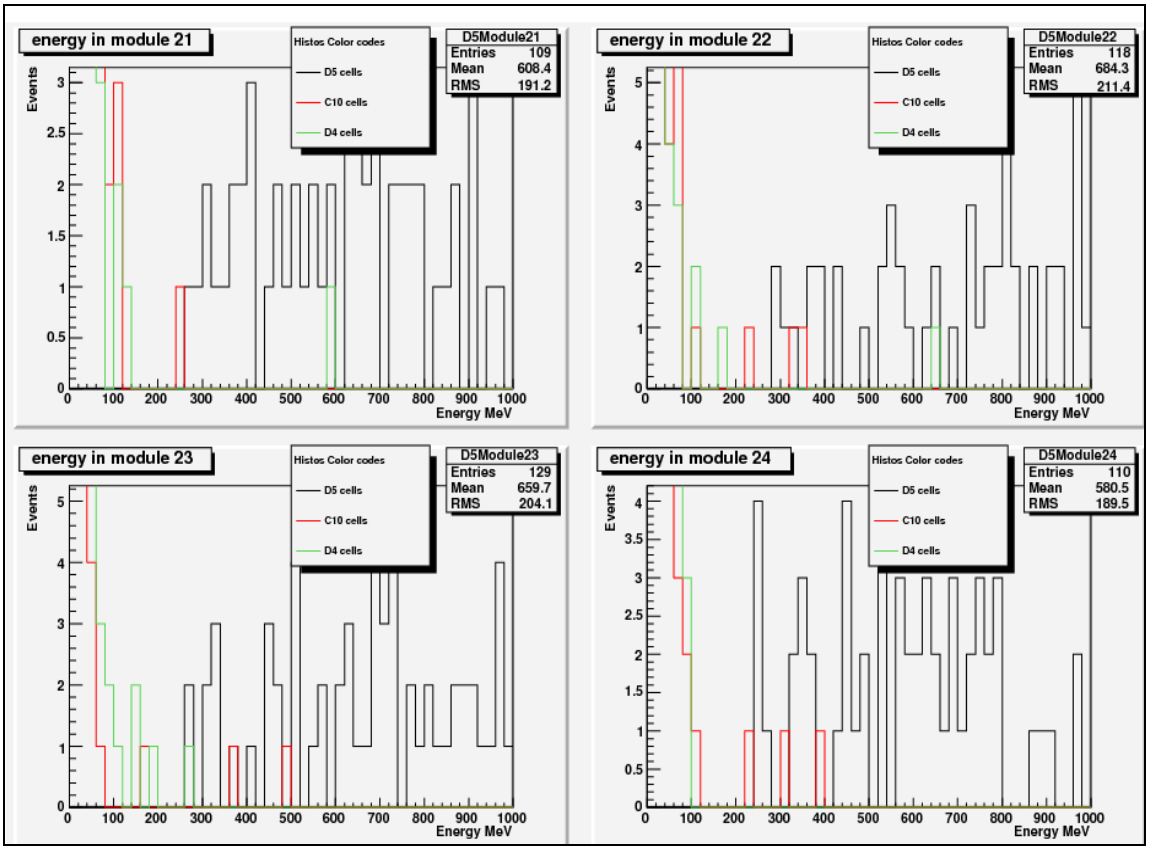

Figure 4.11 D4, D5 and C10 cell response to cosmic muons for 4 adjacent top modules.

Finally we plot the D5 cells energy in black, the D4 energies in red and C10 energies in green. We have cut the plot at energy of 1GeV because, in most of the cases, neither D4 cells, nor C10 cells achieve energies larger than 1GeV; D5 on the other hand has entries up to 4GeV due to its larger size.

There is another important feature we should discuss; the D5 cells have energy depositions that are always than 200 Mev. In this plots, we have not applied a minimum energy cut, so we can clearly see how the “TMF” takes care of the low energy deposition cells produced by noise. Nevertheless because ITC are not included into the “TMF” algorithm, we should not forget about this low energy deposition noise (or background) in the following analysis.

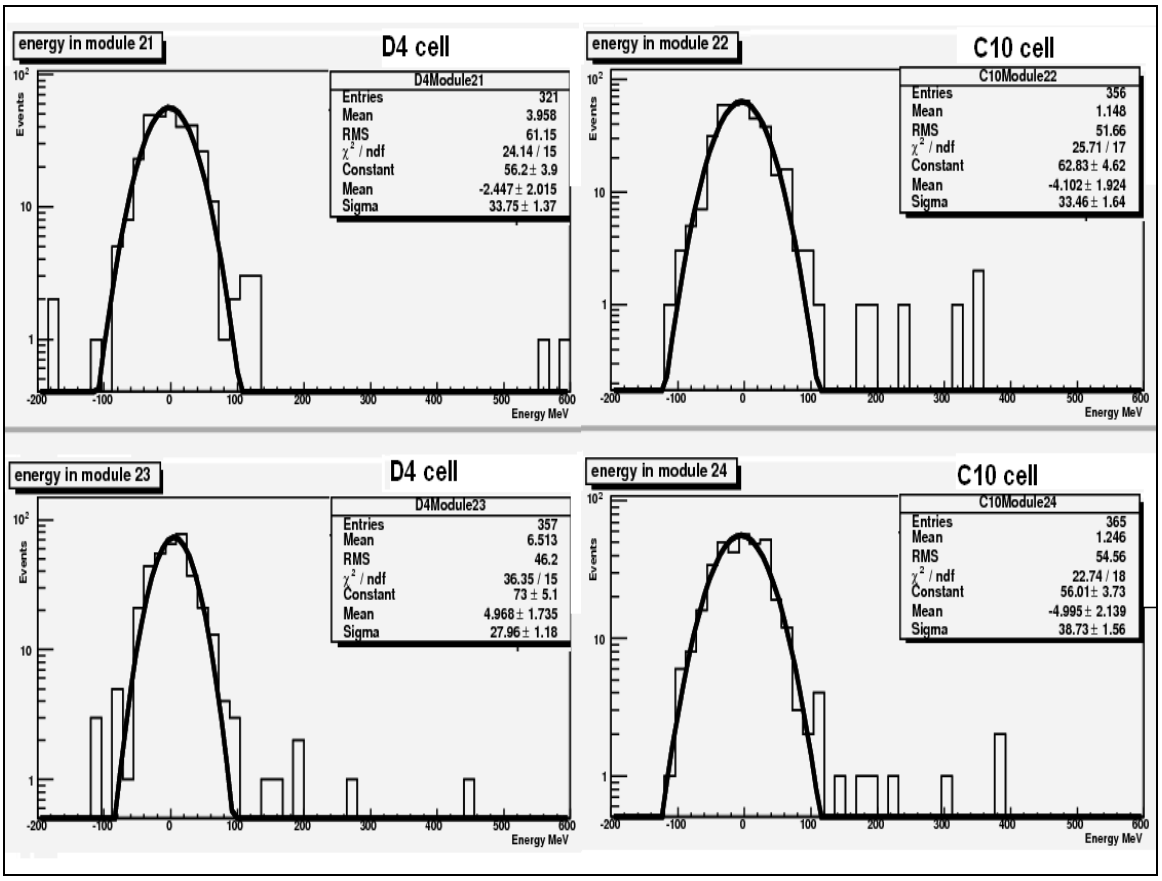

Figure 4.12 ITC cells energy distribution.

Figure 4.12 shows some examples of individual ITC cell's energy distribution. The plots have the same information of those in Figure 4.11, but here they are shown for individual cells and the y axis is in a logarithmic scale. In this way we will able to distinguish the high energy muon signal from the background. We have fitted all the histograms with a Gaussian function and selected the events with energies beyond a three sigma value (most of the time this value is around 120 Mev) as our muon signal. As we can see in Figure 4.12 there is always detection of cosmic muons on the ITC cells. Other modules that are not shown here, present the same value on the 3 sigma level an approximated 5 to 6 entries on average beyond that value. We intend to increase the statistics when other M7 datasets are available, so we can include them into this study.

We have done an additional study, where we forced the muon track to pass through the centre of the detector. In this way we are selecting tracks with an artificial projectivity. We have made a selection on the y=0 plane intersection where |x| and |z| are less than 500 mm (see Figure 4.9). We also select events with energy deposition on the cells D5, and we read information for D4 and C10 energies which correspond to the same D5 module. We also read information of the total energy deposited by the whole muon track in the TileCal. If the D5 energy contribution to the total is large enough we print the information. The results are shown in Table 4.6.

Table 4.6 Energy contribution to the muon track

Event Number	26295		48508		86565		89558	
Energy D4 (MeV)	96	411	27	6	28	177	51	20
Energy C10 (MeV)	52	76	41	31	2	20	23	50
Energy D5 (MeV)	1006	101608	1178	8428	30106	1253	19472	13159
Total Track Energy (Mev)	104952		62697		31359		34625	

We have 60 events out of 10000 that passed the selected criteria. We only include in Table 4.6 such events where the contribution on energy deposition coming from D5 is large enough to conclude that the muon track mainly interacted with that specific cell. The fact that it also projective, will assure that it had to pass also through either D4 or C10 cell. Unfortunately by doing this, we reduced the total events from 60 to only 4. Nevertheless those 4 events always have two different D5 cells involved, probably from two adjacent modules or from back to back events, so we will have 8 entries in total. We found that the energy contribution associated to cells D4 and C10 on all 8 entries, is also large enough when combined (more than 3 sigma in Figure 4.12) to be considered a successful cosmic detection.

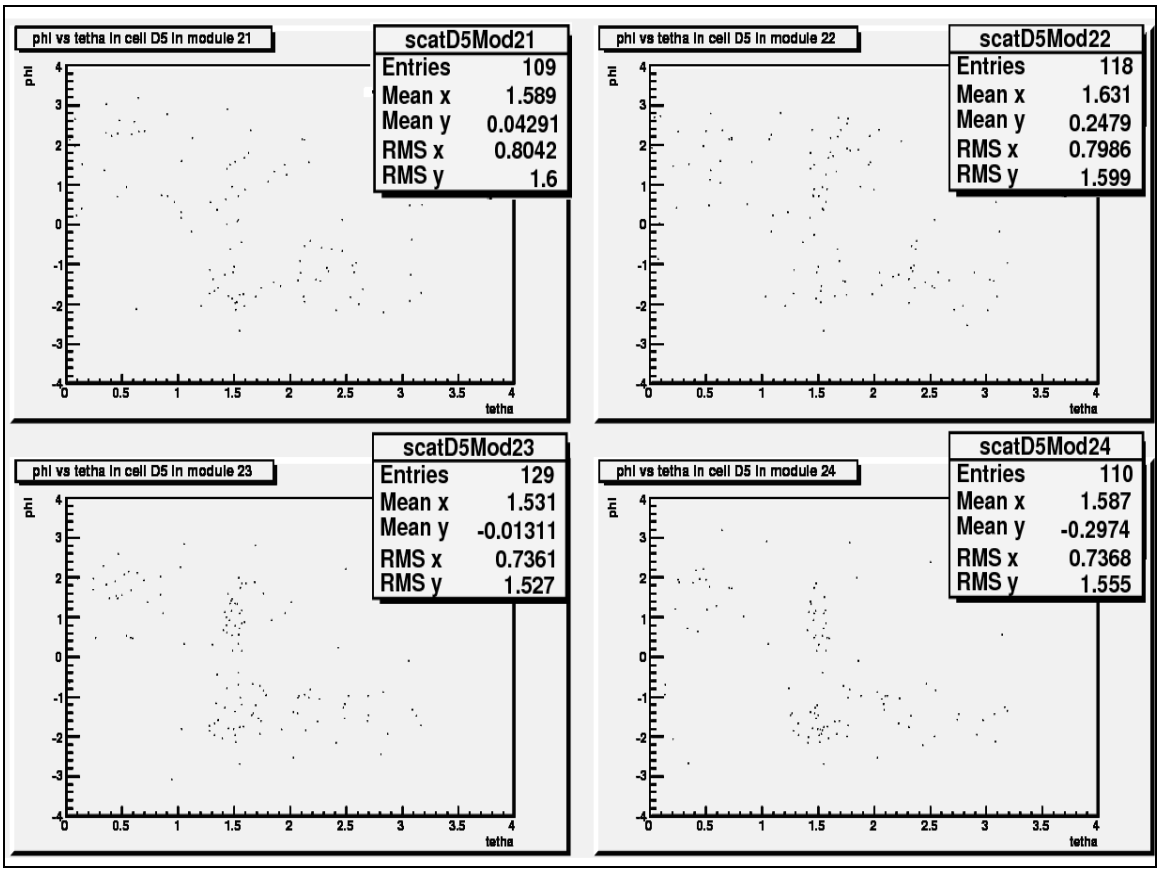

Figure 4.13 Phi Vs. Theta distribution of muons tracks in D5 module.

Finally we present in Figure 4.13 the phi vs. theta distribution of the muon track that was detected by D5 cells in different modules. We can see that the tracks tend to populate the θ=1.5 radians region which represents cosmic rays travelling at an angle of 90 degrees approximately or from top to bottom of the detector. Also the regions $1.5<\Phi<2.5$ and $-2.5<\Phi<-1.5$ corresponding to modules 15 to 25 (top) and 45 to 55 (bottom) respectively, present higher activity, as it is expected.

CHAPTER 5

DILEPTON INVARIANT MASS DISTRIBUTION IN SUSY SIMULATION

This chapter presents results on the reconstruction of dilepton invariant mass using MSUGRA's simplest decay chain where a P-P collision produces a neutralino plus two opposite sign leptons plus quarks in the final state. The analysis was performed with the latest ATHENA software package, SUSYView 11.0.4. The goal is to improve the previous results produced by the ATLAS Data Challenge (DC1) group [15]. This study will focus in the calculation of the invariant mass, using the latest data available from the Monte Carlo datasets available at BNL.

5.1 Experimental Signatures

We first present the most common SUSY processes that could be produced by the LHC, and seen by ATLAS detector. The signature to be studied comes from the MSUGRA scenario. Figure 5.1 shows one possible decay chain.

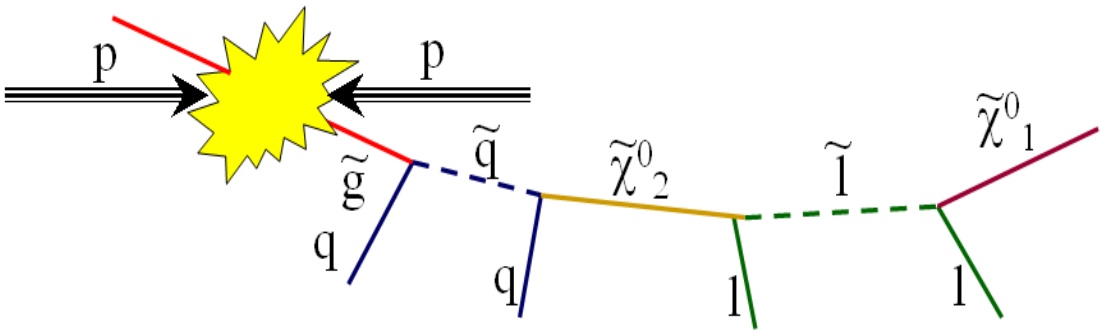

Figure 5.1 Msugra decay chain.

In this case, the two protons coming from opposite sides of the LHC's tunnel collide at the energy of 7 TeV each, head to head, and a SUSY Gluino particle is created which will decay immediately into a quark pair; one of the quarks created will decay into a neutralino and then will decay into a dilepton plus missing energy. The signature we are studying is a dilepton signal and is the last decay of the chain shown below in equation 5.1.

$$\tilde{\chi}_2^0 \rightarrow l^{\mp} l^{m} \rightarrow \tilde{\chi}_1^0 l^{\pm} l^{m} \qquad (5.1)$$

The neutralino undergoes a two body decay. One of its final products is the massive (but invisible) LSSP (lightest supersymmetry particle), which happens to be stable.

The data was created using Monte Carlo code in the Athena software environment. It was analyzed and plotted with ROOT (An object oriented data analysis framework), which allows us faster data storage accessibility. All of the variables corresponding to the particles (example: transverse momentum, number of particles, missing energy etc.) were stored in ROOT Ntuples.

5.2 Data Analysis

The ATLAS Data Challenge 1 studied the dilepton invariant mass in the year 2001 working with an ATHENA version 7.0.2. Their work will be described in detail and their results will be shown. We will reproduce these results with new data and a new version of SUSYView (with the Athena release 11.4.0).

The current analysis is based in the same MSUGRA framework used by the DC1 group, more specifically the "SUGRA Point-5" which is explained in the ATLAS Detector and Physics

Performance TDR [1]. This model allows reduction of the number of free parameters from 110 to around 20. The main parameters are shown in Table 5.1

Table 5.1 Msugra at point 5 parameters.

Parameter	Description	Value
m_o	Unification all scalar masses at GUT scale	100 GeV
$M_{1/2}$	Unification of all neutrino masses at GUT scale	300 GeV
Sign μ	Super potential: $\mu H_1 H_2$	positive
A_0	Tri-linear term	-300 Gev
Tan β	ν_1/ν_2	6
M_H	Higgs mass	115 MeV

The first step, to reconstruct the “SUSY mass scale”, is to obtain the peak value of the invariant mass distribution in the final state of the processes such the one in Figure 5.1. This decay chain has a particular signature. Its final product is always a lepton pair with same flavor but have opposite signs of charge. This is a consequence of the fact that the invariant mass is constrained kinematically.

The invariant mass distribution of the two charged leptons is expected to have a triangular shape with an edge around 100 GeV. The edge can be calculated using equation 5.2.

$$M_{ll}^{max} = M_{\tilde{\chi}_2^0}\sqrt{1-\frac{M_{\tilde{l}}^2}{M_{\tilde{\chi}_2^0}^2}}\sqrt{1-\frac{M_{\tilde{\chi}_1^0}^2}{M_{\tilde{l}}^2}} = 100.31 GeV \qquad (5.2)$$

The M's stands for the different masses of the different particles that have participation in the process of Figure 5.1 the exact result after calculation is 100.31 Gev. This is the value that should be recovered after the simulation is performed.

The dilepton process has four different branches: two electrons (actually a positron and an electron), two muons (again they should be different charge) or positron-muon and antimuon-electron. The last two can be categorized as the same kind so we only have to reproduce a plot for three different dilepton pairs.

The different plots are shown in Figure 5.2. The color convention is the following: The e+e- histogram is plotted in blue, the μ+μ- histogram is plotted in black and the e +/- μ-/+ is plotted in red.

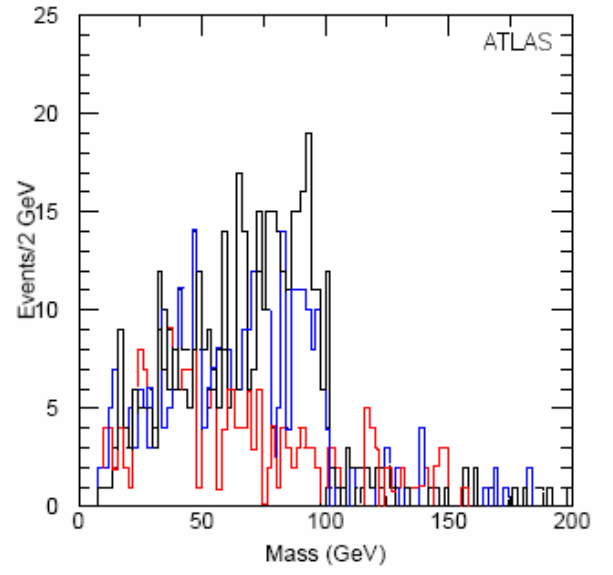

Figure 5.2 lepton signals for e+e- (blue), μ+μ- (black) and e+/-μ-/+ (red).

Finally, the combinatorial background from the dileptons, coming from uncorrelated SUSY decays, can be calculated with equation 5.3.

$$M_{ll}^{max} = \beta^2 M\left(e^{\pm}e^{m}\right) + M\left(\mu^{\pm}\mu^{m}\right) - \beta M\left(e^{\pm}\mu^{m}\right) = 100.31 Gev \qquad (5.3)$$

The scale factor B is 1.22 and is included to account for the difference in the Monte Carlo reconstruction efficiency. This value can be calculated taking the average of the ratio between the number of entries in the e+e- histogram and the μ+μ- histogram from the truth Ntuples. The flavor subtraction allows removal of the standard model background due to different processes not related with SUSY. After this process is done the triangular shape becomes sharper at the specified mass as shown in Figure 5.3.

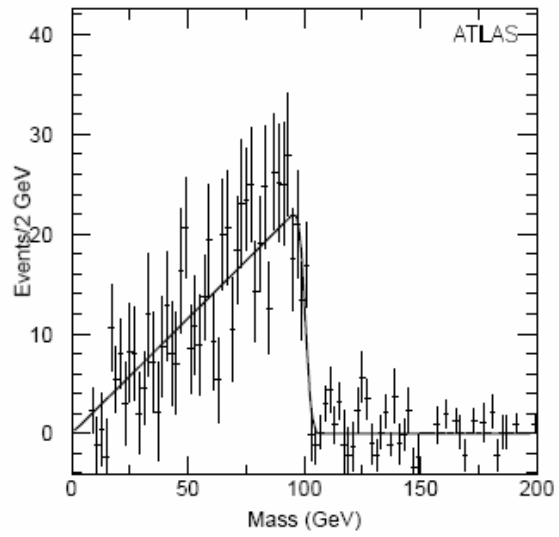

Figure 5.3 Dilepton invariant mass after flavor subtraction.

5.3 Results

The dataset used in the new analysis was taken from the SUSYView group data available at the common area at BNL (Brookhaven national laboratory) at "/usatlas /groups /SUSY /swt2 /Msugra/ hightptview /trig /user/nurcan". These Ntuples were generated by Dr.Nurcan Ozturk, who is a

member of the UTA HEP group. The three TTrees available belong to the SU3 sample. They are: RECO Root, THRU.root and Fast sim. We have worked with the reconstruction information and with the truth information and compared both of them.

The selection cuts for the reconstructed Ntuples (reco) are taken from [16] and they are presented below:

- Only soft electron and soft muons: El_author !=2, Mu_author !=2
- Isolation energy cut on electrons : El_Et_cone<=5000 MeV
- Isolation energy cut on muons: mu_Et_cone<=5000 MeV
- Track match χ^2 positive for muons : Mu_matchChi2>0

The histograms for the dialepton invariant mass created with the reco Ntuples are presented in Figure 5.4

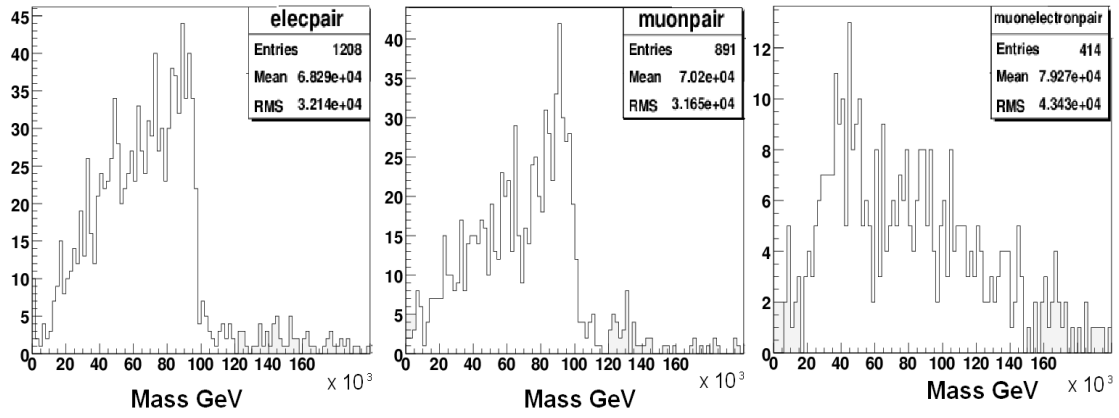

Figure 5.4 Reconstructed signals for for e+e- (left), μ+μ- (center) and e+/-μ-/+ (right).

We can use the truth Ntuples in order to create similar histograms. For the truth information only one condition was required. We selected processes where the two leptons decayed directly from

SUSY particles. Like the neutralino and the Slepton, as it can be seen in Figure 5.1 from the SUSY decay chain. The results for the truth signals are shown in Figure 5.5

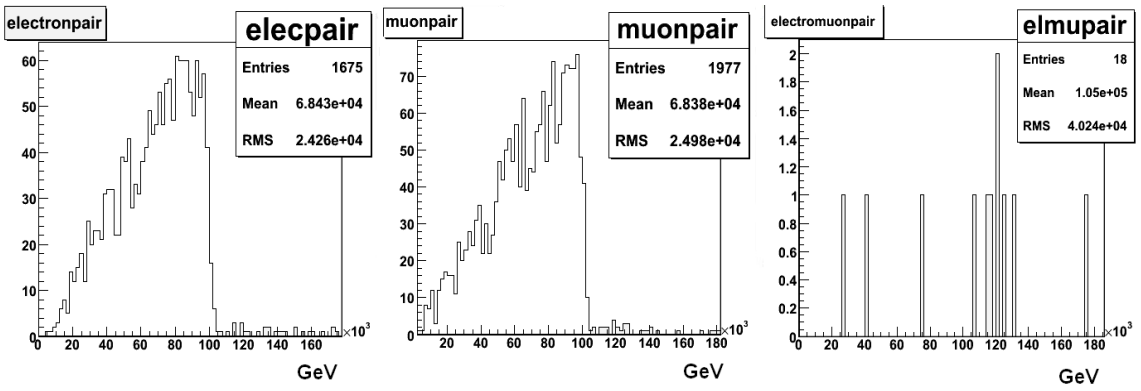

Figure 5.5 Truth signals for for e+e- (left), μ+μ- (center) and e+/-μ-/+ (right).

The plots are shown in different histograms, so that they can be compared with the previous results. We can see how the Truth events for opposite flavor, opposite sign are almost not present as expected, (these signals are background on reco events).

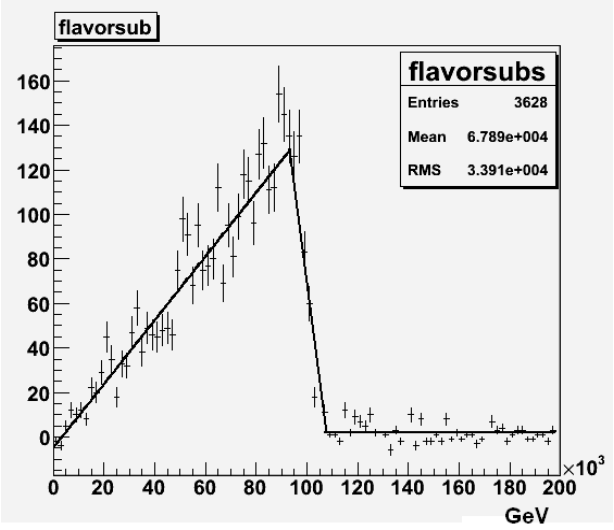

Figure 5.6 Flavor subtraction with the new data.

So far, some improvements can be seen, as the increase in the numbers of events; in this case around 800 in average, also the error bars' size is reduced. Figure 5.6 shows the flavor subtraction of the histograms for the reconstructed events. The edge point is recovered fitting the histogram with a triangular function. The edge point is 100 ±1.10 GeV, in agreement with the theoretical value. The previous result found in [1] is 100 ± 2.1 GeV. The new results present an improvement in the error values due to the increase in the event number.

CHAPTER 6

CONCLUSIONS

The commissioning process of the Atlas detector has taken more than 7 years. UTA has been actively involved in this process with the design, installation and performance analysis of the Intermediate Tile calorimeter cells. We have presented part of this process in this work as my personal contribution, but many other UTA students have been or are still working in this global cooperation. Thanks to this effort, we are very close to complete this commissioning process and eager to see the first run of the LCH and the Atlas detector in December of 2009.

We have presented a detailed description of the analysis performed on the ATLAS ITC cells. We showed the response of the ATLAS ITC cells to energy deposition by cosmic rays and compared it to the response of other Non-ITC cells. Two cosmic rays datasets were used, applying different methodologies on each one of them, we found many events, were it was clear a high energy deposition in the cells under study. These high energy events are at least 3 sigma times over the background signal, on all the modules from both partitions. We can conclude that ITC cells are correctly detecting cosmic rays. Nevertheless we are unable to provide any quantitative information as, detection efficiency, or calibration studies, due to the non-projective nature of cosmic rays and the poor amount of statistics. This kind of information can be calculated when “beam on” datasets are available.

Many of the results presented in this job represent an effort to revalidate and improve previous results in SUSY analysis that we expect to validate at the ATLAS detector. All of the results and work necessary to simulate the future data, provided by the ATLAS detector, will show us and

teach us how to evaluate the real data. The SUSY theory and in special the mSugra model, as we have seen, is a very complex and extensive theory. The work that all the different SUSY groups perform will hopefully corroborate the theory. Once this task is done, a new frontier will be open where many of the new physics will start to play one of the most important roles in understanding the origin of the universe.

REFERENCES

[1] ATLAS Collaboration. *ATLAS detector and physics performance: Technical Design Report*, volume 2. 1999. CERN-LHCC-99-015.

[2] ATLAS Collaboration. *ATLAS tile calorimeter technical design report*, volume1. 1996. CERN-LHCC-96-42.

[3] *Particle Data Group*. Particle physics booklet, July 2006.LBL-61033

[4] D. Griffiths, *Introduction to Elementary Particles*, John Wiley & Sons, 1987ISBN 0-471-60386-4.

[5] ATLAS Collaboration. *ATLAS Liquid Argon Calorimeter: Technical Design Report*. 1996. CERN-LHCC-96-041.

[6] ATLAS Collaboration. *ATLAS muon Spectrometer: Technical Design Report*. 1997. CERN-LHCC-97-022.

[7] ATLAS Collaboration. *ATLAS Magnet System: Technical Design Report, 1*. 1997. CERN-LHCC-97-018.

[8] D. Perkins, *Introduction to High Energy Physics,* Cambridge University Press, 1999ISBN 0-521-62196-8.

[9] A. Ruiz. D*evelopment of a Low pt muon lvl2 Trigger Algorithm with the ATLAS Tilecal Detector*. 2006

[10] F. Varela. *The Detector Control System of the ATLAS experiment at CERN: An application to the calibration of the modules of the Tile Hadron Calorimeter.* 2006

[11] V. González *et al.* Data acquisition in TileCal/ATLAS experiment. Design of the Optical Multiplexer Board Prototype. IEEE Nuclear Science Symposium Conference Record, November 2005.

[12] B. Gosdzik *Comparison of Calorimeter Signals with Trigger Signals at the ATLAS Experiment*, 2007. HD-KIP-07-03.

[13] Athena. *The ATLAS Common Framework. Developer Guide*. 2004.

[14] B. Schumm, *Deep Down Things: The Breathtaking Beauty of Particle Physics*, Johns Hopkins University Press, 2004 ISBN 0-8018-7971.

[15] M. Biglietti et al., *Full Supersymmetry Simulation for ATLAS in DC1*, ATL-PHYS-2004-011 (2004)

[16] A. Barr., *Studies of Supersymmetry Models for the ATLAS Experiment at the Large Hadron Collider.* Churchill College. 2002

[17] ATLAS Collaboration. *Expected Performance of the ATLAS Experiment Detector, Trigger and Physics*. 2008. CERN-OPEN-2008-020.

[18] I. Niessen., *Supersymmetric Phenomenology in the mSUGRA Parameter Space.* The Institute of Mathematicss, Astrophysics and Particle Physics at the Radboud University of Nijmegen. arXiv:0809.1748v1 [hep-ph]. 2008

[19] J. Garvei *et al. The ATLAS Level-1 Calorimeter Trigger Architecture*. IEEE Transactions on Nuclear Science, vol. 51, no. 3, june 2004

[20] https://twiki.cern.ch/twiki/bin/view/Atlas/TileMuonFitter

BIOGRAPHICAL INFORMATION

Carlos Francisco Medina Hernandez was born in Bogota, Colombia, in 1981. He earned his B.E in electrical engineering in 2003 from Universidad de los Andes, Colombia. Two years later he got his B.E in physics from the same university. In spring 2002 he completed the requirements for M.S in physics at University of Texas at Arlington (UTA). Carlos Medina research interests are high energy physics and data analysis. He expects to become a successful researcher and physics professor.